

# Krüppel-like factor gene function in the ctenophore *Mnemiopsis leidyi* assessed by CRISPR/Cas9-mediated genome editing

Jason S. Presnell\* and William E. Browne<sup>‡</sup>

## ABSTRACT

The Krüppel-like factor (Klf) gene family encodes transcription factors that play an important role in the regulation of stem cell proliferation, cell differentiation and development in bilaterians. Although Klf genes have been shown to specify functionally various cell types in non-bilaterian animals, their role in early-diverging animal lineages has not been assessed. Thus, the ancestral activity of these transcription factors in animal development is not well understood. The ctenophore *Mnemiopsis leidyi* has emerged as an important non-bilaterian model system for understanding early animal evolution. Here, we characterize the expression and functional role of Klf genes during *M. leidyi* embryogenesis. Zygotic Klf gene function was assessed with both CRISPR/Cas9-mediated genome editing and splice-blocking morpholino oligonucleotide knockdown approaches. Abrogation of zygotic Klf expression during *M. leidyi* embryogenesis resulted in abnormal development of several organs, including the pharynx, tentacle bulbs and apical organ. Our data suggest an ancient role for Klf genes in regulating endodermal patterning, possibly through regulation of cell proliferation.

**KEY WORDS:** Ctenophore, Krüppel-like factor, KLF5, Endoderm, Evolution, Lithocyte

## INTRODUCTION

Members of the Krüppel-like factor (Klf) gene family encode transcription factors with a characteristic DNA-binding domain composed of three C-terminal C2H2-zinc fingers (McConnell and Yang, 2010; Presnell et al., 2015). During metazoan diversification, the Klf transcription factor gene family expanded via duplication and domain-shuffling events (Presnell et al., 2015). Klf transcription factors are expressed in a variety of cells and tissues and have roles in many biological processes, including proliferation of stem and progenitor cells, embryonic development, germ layer differentiation, neuronal growth and regeneration, immune system regulation and metabolic regulation (Bialkowska et al., 2017; McConnell and Yang, 2010; Moore et al., 2009; Nagai et al., 2009; Oishi and Manabe, 2018; Pearson et al., 2008; Sweet et al., 2018).

Although KLF functional studies have been restricted to bilaterians, Klf genes are found in the genomes of all metazoans (Presnell et al., 2015), with a number of homologs expressed in multipotent stem cells (Tarashansky et al., 2021). Within Cnidaria,

Klf genes are expressed in multipotent interstitial stem cells and their various downstream lineages, as well as in ectodermal epithelial stem cells in *Hydra vulgaris* (Hemrich et al., 2012; Levy et al., 2021; Siebert et al., 2019). In cnidarian single cell RNA-sequencing (RNA-seq) datasets, Klf genes are expressed in various cell types, including gastrodermis, neuronal and gland cell lineages (Levy et al., 2021; Sebé-Pedrós et al., 2018a). In *Hydractinia symbiolongicarpus*, Klf genes are upregulated in male sexual polyp bodies versus female sexual polyp bodies (DuBuc et al., 2020). Within Porifera, Klf genes are expressed in the stem cell-like archaeocytes, epithelial pinacocytes and mesenchymal cells in both *Spongilla lacustris* and *Amphimedon queenslandica* (Musser et al., 2019 preprint; Sebé-Pedrós et al., 2018b). Single cell RNA-seq data for the placozoan *Trichoplax adhaerens* revealed a single Klf gene expressed in epithelial cells (Sebé-Pedrós et al., 2018b). In ctenophores, three Klf genes have been identified in two distantly related species, *Pleurobrachia bachei* and *Mnemiopsis leidyi* (Presnell et al., 2015). The genome of *M. leidyi* contains *Klf5a*, *Klf5b* and *KlfX* (Presnell et al., 2015). *Klf5a* and *Klf5b* are the result of a lineage-specific duplication within the Ctenophora, whereas *KlfX* is highly derived with no clear orthology to any known metazoan Klf clade (Presnell et al., 2015). To date, single cell and tissue-specific RNA-seq studies in *M. leidyi* have not established differential expression signatures for Klf genes (Babonis et al., 2018; Sebé-Pedrós et al., 2018b).

*M. leidyi* is a species of the non-bilaterian phylum Ctenophora, one of the earliest-diverging extant metazoan lineages (Dunn et al., 2008; Hejnol et al., 2009; Kapli and Telford, 2020; Li et al., 2021; Shen et al., 2017; Whelan et al., 2017). *M. leidyi* has been used extensively as a model for investigating early metazoan developmental patterning, regeneration and the evolution of animal traits (Babonis et al., 2018; Bessho-Uehara et al., 2020; Fischer et al., 2014; Martindale and Henry, 1999; Presnell et al., 2016; Reitzel et al., 2016; Salinas-Saavedra and Martindale, 2020; Schnitzler et al., 2014; Yamada et al., 2010). *M. leidyi* embryos undergo a ctenophore-specific early cleavage program, with gastrulation taking place ~3-5 h post-fertilization (hpf), followed by tissue organization and organogenesis over the next several hours (Fischer et al., 2014; Freeman, 1976; Fig. 1A). Four pairs of ctene rows, one pair in each quadrant, are typically among the first differentiated ectodermal structures to appear (Fischer et al., 2014). Each ctene plate is made up of polster cells bearing fused giant cilia (Tamm, 1973). Whereas initial ctene plate development is established by maternal factors (Fischer et al., 2014), new ctene row expansion begins post-hatching during the juvenile cydippid stage (Tamm, 2012). After the formation of the initial ctene rows, the developing embryo rapidly increases in size. This period of rapid growth is accompanied by pharynx elongation along the aboral/oral axis, the development of tentacle bulbs, and deposition of the first lithocytes onto the balancer cilia of the apical organ (Martindale and Henry, 2015). Lithocytes are mineralized cells that form a statolith

Department of Biology, University of Miami, Cox Science Center, 1301 Memorial Drive, Miami, FL 33146, USA.

\*Present address: Department of Human Genetics, University of Utah, 15 N 2030 E, Salt Lake City UT 84112, USA.

<sup>‡</sup>Author for correspondence (w.browne@miami.edu)

 J.S.P., 0000-0002-7225-6692; W.E.B., 0000-0001-8200-6489

Handling Editor: Cassandra Extavour  
Received 1 May 2021; Accepted 26 July 2021

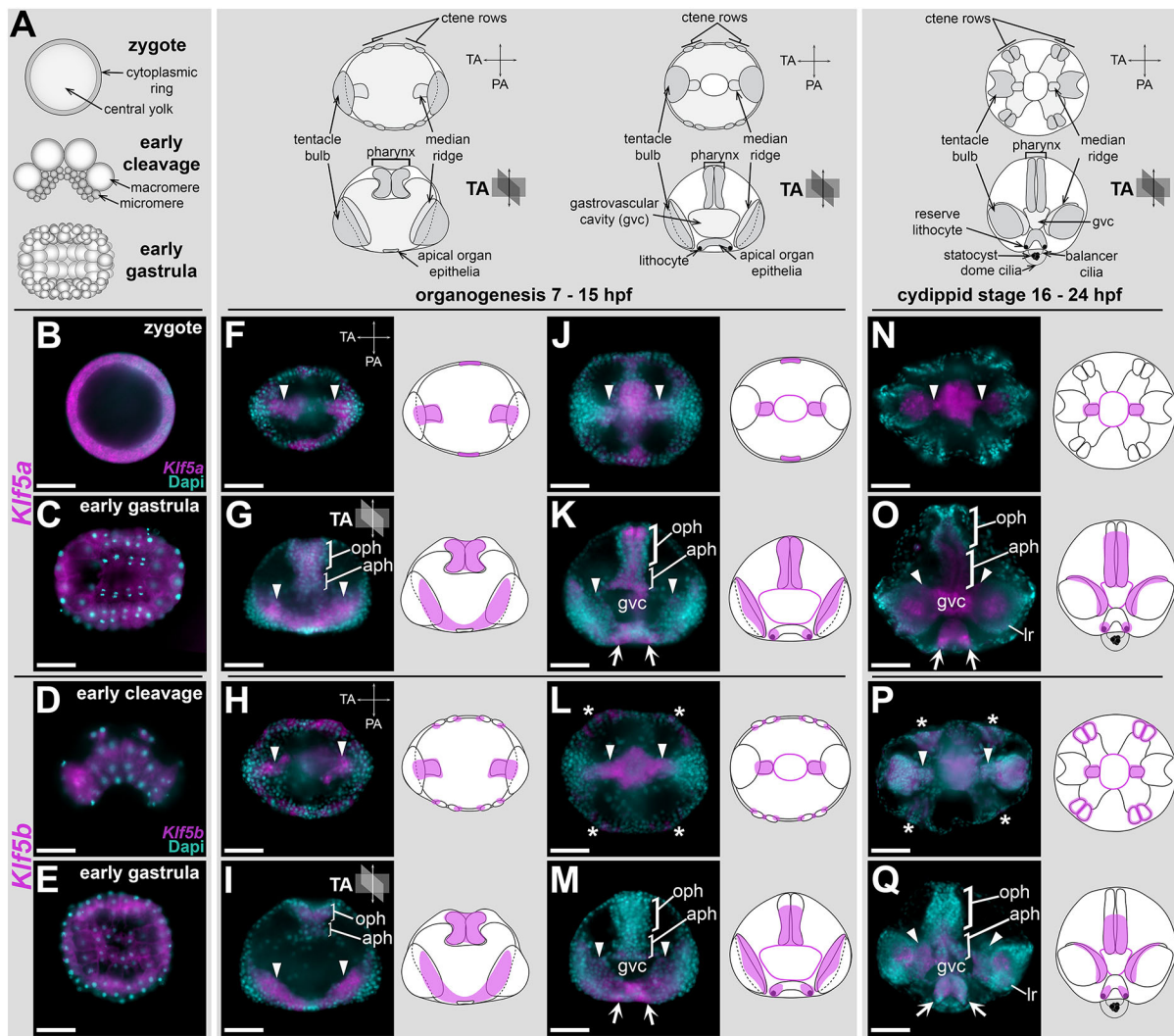


**Fig. 1. Zygotic *Kif5a* and *Kif5b* are primarily expressed in endoderally derived tissues during embryogenesis in *Mnemiopsis leidyi*.** (A) Schematics highlighting major morphological landmarks (e.g. ctene rows, pharynx, tentacle bulbs and apical organ) during *M. leidyi* embryogenesis. Gastrulation typically occurs within 6 h post-fertilization (hpf), followed by rapid tissue remodeling and organogenesis over the next several hours. By 24 hpf embryos are ready to hatch as cydippid larvae and have fully developed organ systems. For post-gastrulation embryos, the top row is an aboral view and the bottom row is a lateral view with the oral side facing up and the aboral side facing down. (B–Q) Whole-mount *in situ* hybridization for *Kif5a* in B,C,F,G,J,K,N,O and *Kif5b* in D,E,H,I,L,M,P,Q during embryogenesis. Orientation follows schematics from A. Aboral views are shown in C,E,F,H,I,L,N,P. Lateral views are shown in D,G,I,K,M,O,Q. (B–E) Maternal transcripts for both *Kif5a* and *Kif5b* are ubiquitously distributed during early development in zygotes (B), early cleavage stages (D) and gastrulae (C,E). One representative image for each gene per stage is shown. (F–Q) Zygotic *Kif5a* and *Kif5b* transcript expression domains with corresponding schematics. (F–I) Initially, expression of *Kif5a* and *Kif5b* zygotic transcripts is localized to the forming tentacular median ridges (arrowheads) and the developing pharynx (oph+aph). (J–M) Later during development, *Kif5a* and *Kif5b* transcript expression is also found in the developing apical organ (arrows) and epithelia of the newly formed gvc. (N–Q) In cydippids, *Kif5a* and *Kif5b* transcripts are found in the tentacular median ridge (arrowheads) and lr, on either side of the apical organ floor (arrows), localized towards the aph and throughout the gvc epithelium. (L,P) *Kif5b* transcripts are also expressed in an additional domain around the ctene rows (asterisks). See also Fig. S1A,B. Scale bars: 50  $\mu$ m. aph, aboral end of the pharynx; gvc, gastrovascular cavity; lr, lateral ridge; oph, oral end of the pharynx; PA, pharyngeal axis; TA, tentacular axis.

housed within the apical organ, which functions to control orientation in the water column by coordinating ctene row beating (Jokura and Inaba, 2020; Tamm, 1973, 2014).

Flanking the apical organ along the tentacular axis (TA), a pair of ectodermal invaginations and internal endodermal cells form the developing tentacle bulb organs and their cognate tentacular lateral and median ridges, respectively (Martindale and Henry, 1997b, 1999). Embryonic and adult tentacle bulb organs contain populations of highly proliferative cells in the tentacular lateral ridge and median ridge tissues that give rise to differentiated colloblast and tentacle muscle cells, respectively (Alié et al., 2011; Babonis et al., 2018; Jager et al., 2008; Schnitzler et al., 2014). Genes

associated with germline development and stemness, including *Piwi*, *Vasa*, *Nanos* and *Sox* homologs, are highly expressed in both the lateral and median ridges of the tentacle bulb, as well as in proliferative cell populations in the developing apical organ and ctene rows, supporting the presence of progenitor cells with stem cell-like properties in these tissues. At ~18–20 hpf, the fully developed *M. leidyi* cydippid hatches and maintains a feeding, pelagic lifestyle before transitioning to the adult lobate body plan ~20 days post hatching (Martindale and Henry, 2015). In adult animals, these progenitor cells play a role in the continuous replacement of lost cells (Alié et al., 2011; Jager et al., 2008; Reitzel et al., 2016; Schnitzler et al., 2014).

Previous investigations into gene function in *M. leidy* used morpholino (MO) oligonucleotide-mediated knockdown or mRNA overexpression methods (Jokura et al., 2019; Salinas-Saavedra and Martindale, 2020; Yamada et al., 2010). Here, we report the first use of CRISPR/Cas9 in *M. leidy* for mutagenesis. We used CRISPR/Cas9 to disrupt the zygotic function of two Klf genes, *Klf5a* and *Klf5b*. We show that disruption of Klf gene expression is associated with the abnormal development of various organs during *M. leidy* embryogenesis due to the loss of specific endodermally derived cell types. Our data provide additional insight into the evolution of Klf gene family function within both the metazoan stem lineage and the early-diverging ctenophore lineage. Our use of CRISPR/Cas9 to disrupt Klf gene expression and the subsequent characterization of the loss of Klf expression on development and tissue patterning in *M. leidy* provide a foundation for future mutagenesis studies in ctenophores.

## RESULTS

### *Klf5a*, *Klf5b* and *KlfX* expression during embryonic development

*Klf5a* and *Klf5b* transcripts are maternally loaded in *M. leidy* (Davidson et al., 2017) similar to maternal loading of a number of Klf genes in other metazoans (Blakeley et al., 2015; De Graeve et al., 2003; Weber et al., 2014). *Klf5a* and *Klf5b* transcripts were detected in all embryonic cells through gastrulation (Fig. 1B-E). Post-gastrulation, transcripts for both *Klf5a* and *Klf5b* became spatially restricted to cell populations associated with the developing pharynx, gastrovascular system, tentacle bulb median ridges, and within the developing apical organ (Fig. 1F-Q).

Within the developing pharynx, *Klf5a* and *Klf5b* expression were initially widespread (Fig. 1G,I). As the pharynx elongated, *Klf5a* and *Klf5b* expression became restricted to the interior-most cell layers of the medial and aboral pharyngeal regions (Fig. 1K,M,O,Q). The aboral-most region of the pharynx includes cells that form the junction with the central gastrovascular cavity, or infundibulum. *Klf5a* and *Klf5b* expression was found throughout the endodermal epithelial lining of the presumptive gastrodermis (Fig. 1J-Q). During the initial development of the aboral apical organ, *Klf5a* and *Klf5b* expression was detected in the apical organ floor epithelia. As the apical organ developed, *Klf5a* and *Klf5b* expression became progressively restricted to cells located along the TA that are positionally correlated with sites of lithocyte formation (Tamm, 2014; Fig. 1K,M,O,Q). Within the developing tentacle bulbs, both *Klf5a* and *Klf5b* were expressed in the tentacular median ridge (Fig. 1F-Q). An additional unique *Klf5b* expression domain was detected in a narrow band of epidermal cells surrounding newly formed ctene row polster cells (Fig. 1H,L,P; Fig. S1A,B).

In contrast to both *Klf5a* and *Klf5b*, *KlfX* expression was restricted to late embryogenesis, first appearing ~16 hpf. Expression of *KlfX* transcripts were localized to a small number of cells within the apical organ (Fig. S1C,D). One group of *KlfX*-expressing cells was located deep within the central epithelial floor of the developing apical organ. These cells were located along the TA and pharyngeal axis (PA), forming a cross-shaped pattern (Fig. S1C). A second shallower group of *KlfX*-expressing cells was located within each quadrant immediately medial of the ciliated grooves in the developing apical organ (Fig. S1D). These *KlfX*-expressing cells correspond positionally with the apical organ lamellate bodies, which may represent putative photoreceptor cells (Horridge, 1964a; Jokura and Inaba, 2020; Schnitzler et al., 2012), suggesting that *KlfX* expression may be associated with light-sensing neuronal cell types in the apical organ.

### CRISPR/Cas9 and splice-blocking morpholino experimental design

To characterize zygotic Klf gene function in *M. leidy*, we used both CRISPR/Cas9 mutagenesis and splice-blocking MOs (sbMOs) to knockdown Klf gene expression independently during embryonic development (Fig. 2). We focused on *Klf5a* and *Klf5b* knockdown experiments, because initial *KlfX* gene knockdown experiments failed to produce obvious morphological phenotypes. Importantly, it has been previously shown that co-expressed KLFs bind to shared downstream regulatory targets, resulting in complex functional outcomes. For example, KLF2, KLF4 and KLF5 have redundant roles in the downstream regulation of *Nanog* (Jiang et al., 2008), KLF2 and KLF4 play redundant roles in regulating attachment between tendon and bone tissue (Kult et al., 2021), whereas competition between KLF1 and KLF3 for binding sites can result in disparate functional outcomes (Ilsley et al., 2017). For this reason, we sought to maximize the efficiency of generating an observable phenotype by performing simultaneous *Klf5a* and *Klf5b* knockdown with both sbMO and CRISPR/Cas9 genome-editing experiments.

We injected single cell embryos with either *Klf5a+Klf5b* sbMOs (KLF-MO embryos) or *Klf5a*-single guide RNA (sgRNA)+*Klf5b*-sgRNA (KLF-Cas9 embryos). Microinjected embryos were allowed to develop to ~20 hpf, stained with vital dyes, live imaged and compared with equivalent late-stage wild-type embryos from the same spawns. We used fluorescence-based vital dyes to mark and follow asymmetries in subcellular components associated with key morphological structures in live animals. For example, MitoTracker fluorescence in whole embryos preferentially marks ctene row polster cells containing giant mitochondria with atypical cristae (Horridge, 1964b). By contrast, LysoTracker fluorescence in whole embryos preferentially marks cells containing yolk and large acidic vacuoles associated with the developing gastrovascular cavity and endodermal canals. After phenotype documentation, live animals were recovered and individually processed for DNA or RNA to validate either CRISPR/Cas9 or MO activity, respectively.

Efficient microinjection of knockdown and knockout reagents requires the mechanical removal of the outer vitelline membrane surrounding the fertilized egg. To determine whether mechanically removing the vitelline membrane had an effect on embryogenesis, we scored the percentage of normal development in embryos that were removed from the vitelline membrane but not injected. There was no significant difference between the percentage of normal development of embryos kept in their vitelline membrane (85%,  $n=161$ ) and those that had their vitelline membrane removed but not subsequently microinjected (80%,  $n=217$ ;  $\chi^2=1.5272$ ,  $P=0.217$ ; Fig. S2A). In addition, microinjections with a standard control MO (79% normal,  $n=49$ ), Cas9 protein alone (86% normal,  $n=7$ ) or with sgRNAs alone (75% normal,  $n=4$ ) also had no detectable effect on embryonic development (Fig. S2A).

We validated gene expression knockdown efficiency by selecting a subset of KLF-MO, KLF-Cas9 and wild-type embryos for single-embryo RNA or DNA analyses post-experimental manipulation. For both *Klf5a* and *Klf5b*, sbMOs produced mRNA splicing errors in KLF-MO embryos via exon skipping and/or intron retention (Fig. 2A,B,E,F). An initial set of four sgRNAs were designed for *Klf5a* and *Klf5b* (Table 1) based on the *M. leidy* reference genome (Moreland et al., 2014, 2020; Varshney et al., 2015). For each gene, a single sgRNA, *Klf5a*-sgRNA4 and *Klf5b*-sgRNA3 (Fig. 2A,E), proved efficient at mediating Cas9 double-stranded break activity at the target loci (Fig. 2C,D,G,H). Sanger sequencing followed by Inference of CRISPR Edits (ICE) analysis (Hsiao et al., 2019

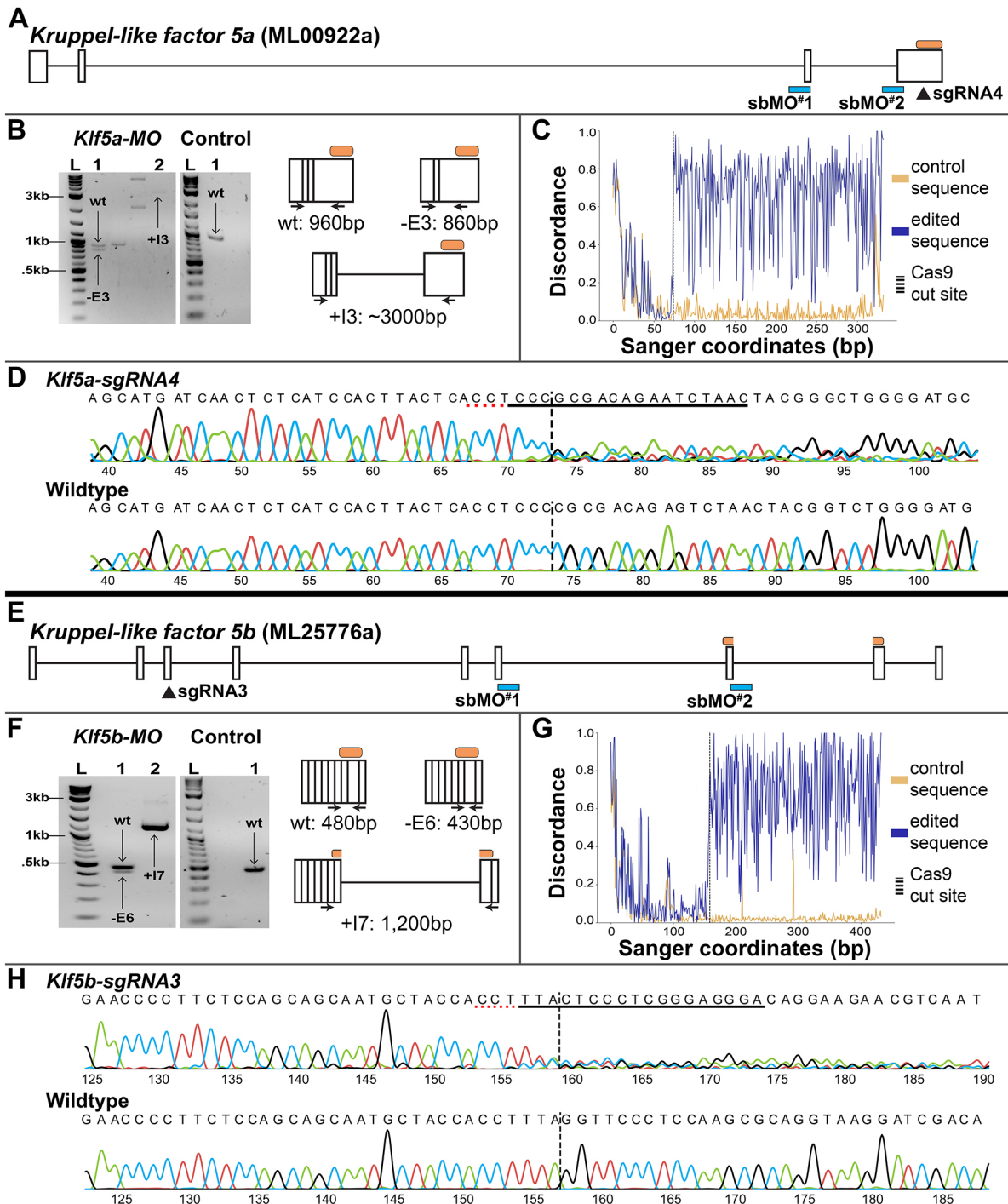


**Fig. 2. Validation of independent methods used to abrogate *Klf5a* and *Klf5b* gene function in *Mnemiopsis leidyi*.** (A,E) *Klf5a* (A) and *Klf5b* (E) exon-intron schematics show the location of sbMO targets (blue boxes) and sgRNA targets (black triangles) used in this study. The orange bars indicate the location of the DNA-binding domain. (B,F) Electrophoretic gels of PCR products obtained using different sets of *Klf5a* and *Klf5b* sbMO RT-PCR primers on cDNA obtained from a single individual KLF-MO embryo exemplar (left) and control embryo exemplar (right). Schematics to the right of the gel images highlight examples of wt amplicon exon skipping (-E) and/or intron retention (+I) amplicons captured with primers for each gene (Table 1). (B) *Klf5a-MO* gel: 2-log DNA ladder (L) was used for band size reference, unlabeled lanes are not relevant to this study. Lane 1 shows both a 960 bp wt and a 860 bp third exon-skipped (-E3) *Klf5a* amplicon. Lane 2 shows a ~3 kb third intron retention (+I3) *Klf5a* amplicon. Control gel: 2-log DNA ladder (L) used for band size reference. Lane 1 shows a single 960 bp wt *Klf5a* amplicon. (F) *Klf5b-MO* gel: 2-log DNA ladder (L) used for band size reference. Lane 1 shows both a 480 bp wt and a 430 bp sixth exon-skipped (-E6) *Klf5b* amplicon. Lane 2 shows a ~1.2 kb seventh intron-retained (+I7) *Klf5b* amplicon. Control gel: 2-log DNA ladder (L) used for band size reference. Lane 1 shows a single 480 bp wt *Klf5b* amplicon. Wild-type and mis-spliced transcripts because of -E and/or +I were present in KLF-MO embryos ( $n=21$  KLF-MO embryos). (C,G) Discordance plots produced using ICE software show elevated sequence discordance downstream of predicted Cas9 cut sites relative to control genomic sequence. (D,H) Corresponding Sanger sequence traces from genomic DNA extracted from a single individual exemplar KLF-Cas9 embryo show signal degradation downstream of the Cas9 cut site compared with a single individual exemplar wt embryo ( $n=17$  KLF-Cas9 embryos). Sanger sequencing signal degradation is caused by the introduction of indels in KLF-Cas9 embryos. The sgRNA target sites are underlined and the positions of the predicted Cas9 cut sites are represented by a vertical dashed line. wt, wild type.

**Table 1. Primers and oligonucleotides used in this study**

Name	Use	Forward	Reverse
<i>Klf5a</i>	ISH probe	ATGAGTGCTATGACATG	AAACGGTTCAAAATGCCTCTT
<i>Klf5b</i>	ISH probe	ATGGAGGTTTCCACGC	AGACGAGCTAGGGGAACG
<i>KlfX</i>	ISH probe	GGCAGTTTAGTTCGATCGG	TGCAGTGAGTGGTAGGTT
<i>Klf5a</i> sbMO1	sbMO	TCTCGTCTGAAACAATTTAAGT	n/a
<i>Klf5a</i> sbMO2	sbMO	GTCTACCCTGCAAGATTTAAGT	n/a
<i>Klf5b</i> sbMO1	sbMO	CAGTTGATTTCTACCTGCCAAGAA	n/a
<i>Klf5b</i> sbMO2	sbMO	CAACAGACTTACCTTCAAATGTGA	n/a
Standard control	sbMO	CCTTACCTCAGTTACAAATTTATA	n/a
<i>Klf5a</i> sbMO RT-PCR	sbMO validation	CCCTTGAAACTTGAAGCA	TCCTTCGTAAACCTTCCG
<i>Klf5b</i> sbMO RT-PCR	sbMO validation	GACAAGTCCAAAGACTAAC	TACAGTAGATGAGGAGGTTT
Universal tracrRNA	sgRNA synthesis	AAAAGCACCGACTGTGCCACTTTTTCAAGTTGATAACGGACTAGCCTATTTTAACTT- GCTATTTAGCTCTAAAC	n/a
sgRNA template	sgRNA synthesis	GAAATTAATACGACTCACATATATA	n/a
<i>Klf5a</i> -sgRNA1	sgRNA synthesis	AGCAACGGTCCGTCCTCGT	n/a
<i>Klf5a</i> -sgRNA2	sgRNA synthesis	TTGAGGACCGGGAGCAA	n/a
<i>Klf5a</i> -sgRNA3	sgRNA synthesis	ACGGAGGAATCGCGCAT	n/a
<i>Klf5a</i> -sgRNA4	sgRNA synthesis	TTAGACTCTGTCGGGGG	n/a
<i>Klf5b</i> -sgRNA1	sgRNA synthesis	TGGTGATATACCAGCGC	n/a
<i>Klf5b</i> -sgRNA2	sgRNA synthesis	ATCTTTCACGCTTAGGGGC	n/a
<i>Klf5b</i> -sgRNA3	sgRNA synthesis	CGCTTGGAGGGAACCTAA	n/a
<i>Klf5b</i> -sgRNA4	sgRNA synthesis	CTGAAACACCCGTCGCAG	n/a
<i>Klf5a</i> -sgRNA4 sequencing	sgRNA/Cas9 validation	AAGACGTCGGATATTTCTCTC	GGTGATCACCTCCTACTGAAA
<i>Klf5b</i> -sgRNA3 sequencing	sgRNA/Cas9 validation	GGTGTTCCATACCTAGACCGAT	TGTGCTGTGTATAGTCGAG

All sequences are oriented 5'-3'. Italicized nucleotide sequences correspond to T7 promoter. Bold nucleotide sequences correspond to genomic Klf targets and include addition of two 5' G residues to aid T7 polymerase binding. Underlined nucleotide sequences denote region of complementarity between templated primers and universal tracrRNA primer, which are annealed to form the sgRNA transcription template.

preprint) revealed a clear degradation of sequence trace signal at the target loci in KLF-Cas9 embryos compared with control embryos (Fig. 2C,G), indicating the presence of indels and putative frameshift mutations generated by sgRNA-targeted Cas9 exonuclease activity (Fig. S2C). ICE analysis also predicted the occurrence of frameshift mutations between ~20-30% (Fig. S2C).

We reduced the chance of potential off-target site (OTS) Cas9-mediated exonuclease activity by designing sgRNAs that had no fewer than three mismatches to nontarget loci in the *M. leidyi* reference genome. To assess potential OTS Cas9 exonuclease activity, we designed primers, amplified and Sanger-sequenced regions around the remaining set of predicted low-probability cut sites of non-KLF genes. No evidence of Cas9 exonuclease activity was observed (Table 2). Thus, we interpreted that phenotypes generated by both gene abrogation approaches in our study resulted from the simultaneous disruption of *Klf5a* and *Klf5b* gene expression.

**Knockdown of zygotic *Klf5a* and *Klf5b* expression**

KLF-MO and KLF-Cas9 embryos phenocopied one another and displayed phenotypes of varying penetrance (Fig. 3A-Q). A higher proportion of severe phenotypes were observed among KLF-Cas9 embryos compared with KLF-MO embryos (Fig. S2B), reflecting the effects of Cas9-mediated genome editing versus titration of functional mRNAs by sbMOs. In contrast to the observation of predominantly severe phenotypes in KLF-Cas9 embryos injected with *Klf5a*-sgRNA4+*Klf5b*-sgRNA3 (Fig. 3P,Q), single-gene knockdown using either *Klf5a*-sgRNA4 or *Klf5b*-sgRNA3 primarily generated mild phenotypes (Fig. S3).

KLF-MO and KLF-Cas9 embryos with mild phenotypes underwent pharyngeal elongation simultaneously with both mesoglea extrusion and a concomitant increase in size similar to that observed in control embryos; however, experimental embryos displayed disorganized patterning at the aboral end of the pharynx and the infundibular gastrovascular cavity (Fig. 3F,G,N,O). Occasionally, we observed pharyngeal bifurcation at the junction of the pharynx with the infundibular gastrovascular cavity (Fig. 3G,O; Fig. S4). By contrast, in severely affected embryos, the internal embryonic space typically occupied by mesogleal extracellular matrix (ECM) was absent and the interior volume was completely occupied by gastrovascular endoderm and abnormally elongated pharyngeal tissue. Thus, embryos with severe phenotypes failed to increase in size, most likely because of the lack of ECM extrusion into the mesoglea space (Fig. 3A,H,I,P,Q). Both the stomodeum and oral regions of the pharynx were still visible in severe mutant embryos, indicating that the entire pharyngeal structure was not lost. However, it is unclear whether the observed abnormal pharyngeal elongation is caused by Klf gene abrogation directly or is a spatial effect due to the absence of mesogleal ECM.

Among both KLF-MO and KLF-Cas9 embryos, patterning defects were also observed in the apical organ (Fig. 3 and Fig. 4A-G). *Klf5a* and *Klf5b* knockdown resulted in a significant reduction in apical organ lithocytes compared with control embryos (Fig. 4A-G). By 20 hpf, control embryo statocysts contained an average of approximately seven lithocytes (Fig. 4A,B,G). KLF-MO embryos had an average of approximately four lithocytes, with three embryos lacking lithocytes entirely (Fig. 4C,D,G). KLF-Cas9 embryos had an average of approximately two lithocytes, with five embryos completely lacking lithocytes (Fig. 4E-G). Notably, both KLF-MO and KLF-Cas9 embryos lacking lithocytes still possessed phenotypically normal balancer cilia and dome cilia, tissues derived from ectoderm (Fig. 4D,F).

**Table 2. Off-target CRISPR/Cas9 loci with mismatches to either *Klf5a* or *Klf5b* target sequence and primers used for Sanger sequencing**

Locus ID	Number of mismatches	Forward	Reverse
ML090223a	4 ( <i>Klf5a</i> -sgRNA4)	AAATTGTTTGTGTTTCACT	AGTTTTCTTTGTTTTTCAGGG
ML021138a	5 ( <i>Klf5a</i> -sgRNA4)	CAGCTTCATTGTAAAGAGTC	TTAGTTCCTATGTTTTTCGCG
ML200217a	5 ( <i>Klf5b</i> -sgRNA3)	GGATACTAGTTCATAGCAG	CTCCTTGTTGATATTCTGGA
ML00363a	6 ( <i>Klf5b</i> -sgRNA3)	TATGATTCTTGTACCAGGG	ACATACGTCATCATTAGC
ML02979a	7 ( <i>Klf5b</i> -sgRNA3)	CTGCATGATTACAAAGGTTT	ATGCTAAGAAGGATGCAATA

All sequences are oriented 5'-3'.

The simultaneous abrogation of *Klf5a* and *Klf5b* also resulted in a dramatic reduction in tentacle bulb size, particularly in the tentacular median ridge (Fig. 3 and Fig. 4H-N). We measured the tentacular median ridge width and found significant differences

between control and injected embryos (Fig. 4N; Fig. S5). The control embryo average tentacular median ridge width was ~23 μm. KLF-MO (Fig. 4J,K) and KLF-Cas9 (Fig. 4L,M) embryo average tentacular median ridge width was ~18 μm and ~9 μm, respectively

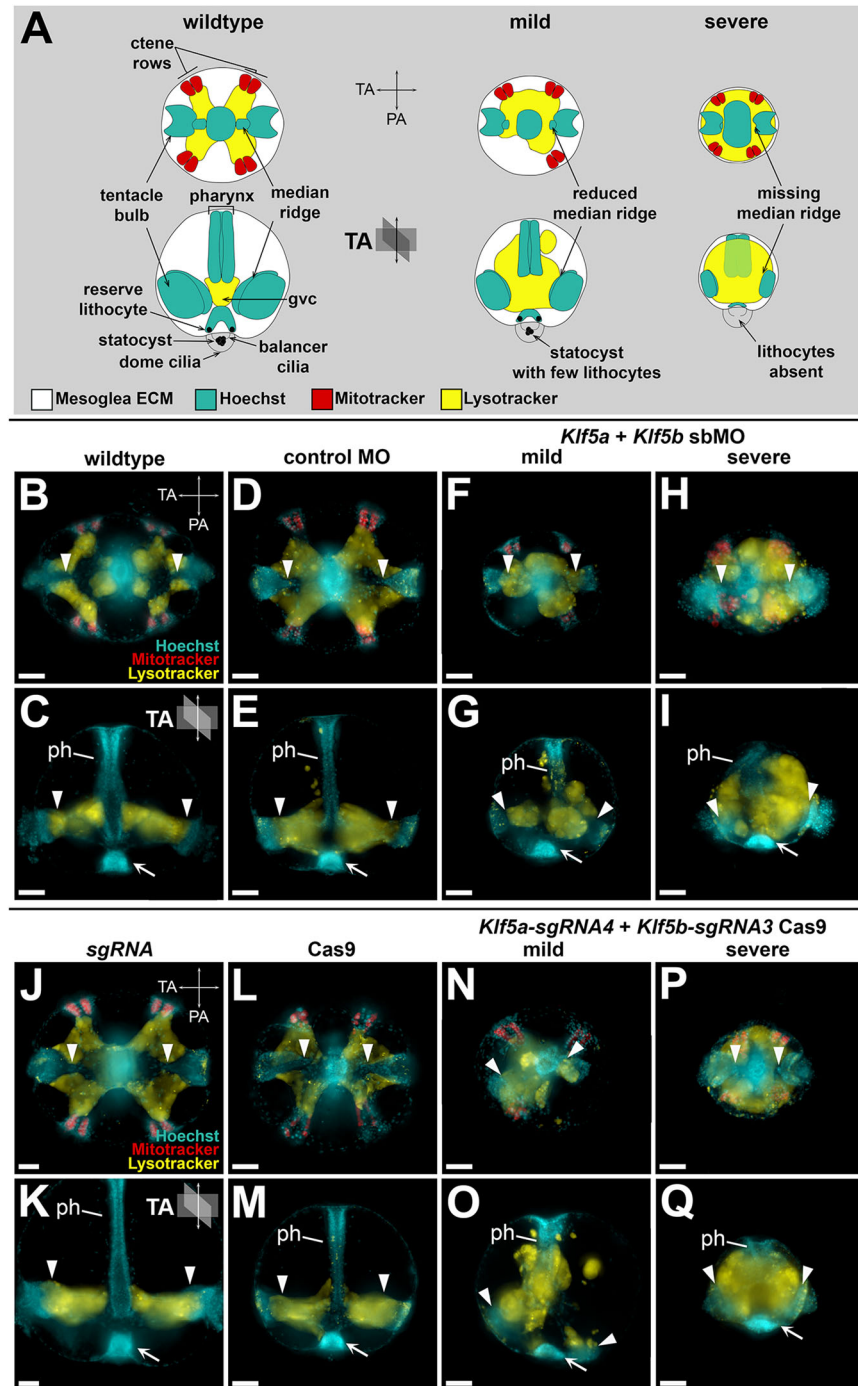


**Fig. 3. Phenotypes generated by *Klf5a* and *Klf5b* double-gene knockdown via sbMO and sgRNA-Cas9 genome editing in *Mnemiopsis leidyi*.** (A)

Representative schematics (see Fig. 1A) of wild-type, mild and severe phenotypes highlighting tissues and cell types disrupted in KLF-MO and KLF-Cas9 *M. leidyi* embryos. The top row is an aboral view. The bottom row is a lateral view with the oral side up and aboral side down. (B-Q) Representative live images of ~20 hpf cydippids. Aboral views are shown in B,D,F,H,J,L,N,P, and lateral views, with the oral side up, are shown in C,E,G,I,K,M,O,Q. TA and PA orientations are as indicated in A. (B,C) Un-injected wild-type embryo. Hoechst (blue) marks nuclei. MitoTracker (red) preferentially marks the position of ctene row polster cells, one pair per embryonic quadrant. Lysotracker (yellow) preferentially stains epithelial cells lining the gvc. Tentacular median ridges (arrowheads) are positioned medially along the TA and contacted by gvc epithelial cells. The ph is positioned centrally and joins with the gvc aborally. The apical organ (arrow) is located at the aboral pole of the embryo. Morphology is unaffected in embryos sham injected with control MO (D,E), sgRNA only (J,K) or Cas9 protein only (L,M). By contrast, mild phenotypes in double-gene knockdown KLF-MO embryos (F,G) and double gene-edited KLF-Cas9 embryos (N,O) display aberrant distributions of gvc epithelial cells (Lysotracker signal), aberrant patterning of the ph, including aboral bifurcations (G,O; see Fig. S4), aberrant patterning of the tentacle bulb and tentacular median ridges (arrowheads), and atypical apical organ (arrow) morphology. Severe phenotypes in double gene-knockdown KLF-MO embryos (H,I) and double gene-edited KLF-Cas9 embryos (P,Q) are reduced in size because of a lack of mesoglea ECM extrusion, display a collapsed ph with gvc junction defects, significantly reduced tentacle bulbs and tentacular median ridges (arrowheads), and apical organ defects (arrow). Scale bars: 50 μm. gvc, gastrovascular cavity; PA, pharyngeal axis; ph, pharynx; TA, tentacular axis.

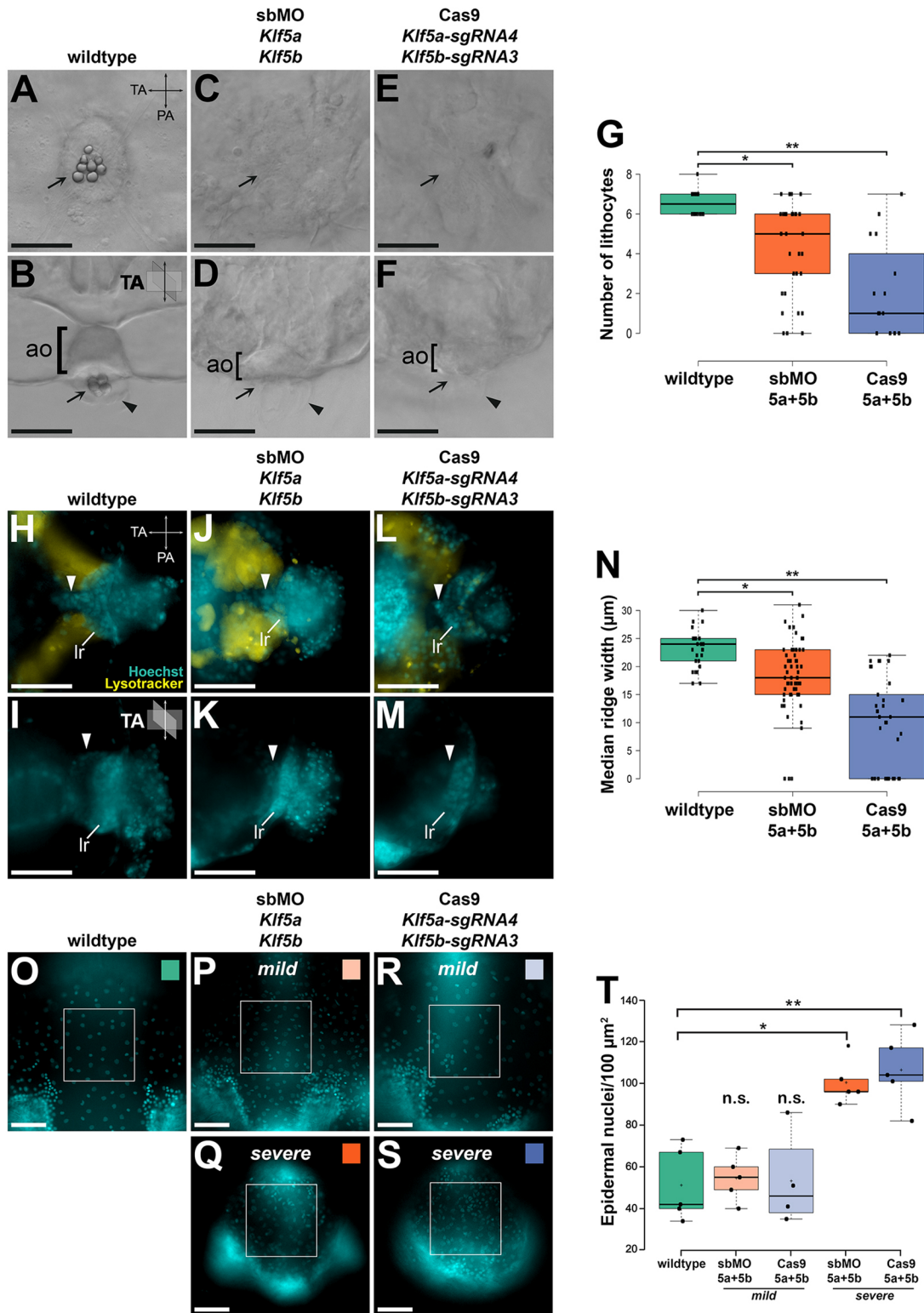


Fig. 4. See next page for legend.

(Fig. 4N). Moreover, we observed that 15% of KLF-MO embryos and 29% of KLF-Cas9 embryos lacked tentacular median ridges altogether (Fig. 4J-N).

In severely affected animals, we observed a significant increase in the density of epidermal cells, ~100 nuclei/100 μm<sup>2</sup> in severe embryos compared with ~50 nuclei/100 μm<sup>2</sup> in wild-type embryos

( $P < 0.005$ ; Fig. 4O-T). The spacing between epidermal cell nuclei was closer among the severe phenotypes relative to normally developing animals (Fig. 4O-S). This suggests reduced lateral tension forces on epidermal cells in animals lacking underlying mesogleal ECM and indicates that the total number of epidermal cells remained the same, with only their spatial relationship being

**Fig. 4. *Klf5a* and *Klf5b* double-gene knockdown disrupts the development of endodermally derived cell types and structures, including lithocytes and the tentacular median ridge.** (A-F, H-M, O-S) Live images of embryos at ~20 hpf. Schematics of TA and PA orientation are in A, B, H, I. Aboral views are shown in A, C, E, H, J, L. Lateral views, with the oral side up, are shown in B, D, F, I, K, M, O-S. (A, B) Wild-type embryo with view of the ao showing the position of lithocytes (arrow) and dome cilia (arrowhead). (C, D) Representative double gene-knockdown KLF-MO embryo and (E, F) representative double gene-edited KLF-Cas9 embryo lacking lithocytes. Dome cilia (arrowheads) and balancer cilia are present in both KLF-MO and KLF-Cas9 embryos. (G) Quantification of lithocyte production. *Klf5a* and *Klf5b* double-gene knockdown significantly reduces lithocyte production. Centerlines show the medians; box limits indicate the 25th and 75th percentiles; whiskers extend 1.5 times the interquartile range from the 25th and 75th percentiles;  $*t=3.47$ ,  $P<0.005$ ;  $**t=6.52$ ,  $P<0.00001$ ; two-tailed unpaired  $t$ -test. Individual counts are plotted as black dots, representing  $n=14$ , 33 and 15 embryos, respectively. (H, I) Wild-type tentacular median ridge (arrowhead) and lr. (J, K) Representative double gene-knockdown KLF-MO embryo and (L, M) representative double gene-edited KLF-Cas9 embryo with dramatically reduced tentacular median ridge. The tentacle bulb lr is unaffected in both KLF-MO and KLF-Cas9 embryos. (N) Quantification of tentacular median ridge width. *Klf5a* and *Klf5b* double-gene knockdown significantly reduces tentacular median ridge width. Centerlines show the medians; box limits indicate the 25th and 75th percentiles; whiskers extend 1.5 times the interquartile range from the 25th and 75th percentiles;  $*t=4.01$ ,  $P<0.0005$ ;  $**t=8.32$ ,  $P<0.00001$ ; two-tailed unpaired  $t$ -test. Individual measurements are plotted as black dots, where  $n=28$ , 61 and 34 tentacular median ridge widths, respectively. Each measurement represents a single tentacular median ridge width, with a maximum of two from each embryo (i.e. an individual embryo has two tentacular median ridges; thus, each embryo may contribute two tentacular median ridge width measurements). A measurement of 0 indicates the absence of a tentacular median ridge and/or tentacle bulb. (O-S) Representative images from a subset of each group of embryos with a  $100\ \mu\text{m}^2$  region of interest focused on the outer epidermal cell layer of wild-type (O), KLF-MO mild (P) and severe (Q) embryos, and KLF-Cas9 mild (R), and severe (S) embryos. (T) Quantification of epidermal nuclei cell counts. Area nuclei counts are plotted as black dots representing  $n=5$ , 5, 4, 5 and 5 area count samples, respectively. KLF-MO severe (mean $\pm$ s.d.:  $100.40\pm 10.7$ ) and KLF-Cas9 severe (mean $\pm$ s.d.:  $106.40\pm 17.4$ ) embryos both had a significantly higher density of epidermal nuclei counts per  $100\ \mu\text{m}^2$  area compared with control embryos (mean $\pm$ s.d.:  $51.20\pm 17.5$ ). There was no significant difference in epidermal nuclei counts for KLF-MO mild embryos (mean $\pm$ s.d.:  $54.60\pm 11.0$ ) or KLF-Cas9 mild embryos (mean $\pm$ s.d.:  $53.25\pm 22.8$ ) relative to control embryos. Centerlines show the medians; box limits indicate the 25th and 75th percentiles; whiskers extend 1.5 times the interquartile range from the 25th and 75th percentiles; crosses represent sample means;  $*t=-5.35225$ ,  $P<0.005$ ;  $**t=-4.99757$ ,  $P<0.005$ ; two-tailed unpaired  $t$ -test. Scale bars:  $50\ \mu\text{m}$ . ao, apical organ; lr, lateral ridge; PA, pharyngeal axis; TA, tentacular axis.

altered (i.e. closer spacing of nuclei). Thus, despite a decreased total body size, the ectodermal cell contribution to the epidermis appeared to be largely unaffected.

The tentacular median ridge in adult *Pleurobrachia pileus* and juvenile *M. leidyi* cydippids has previously been shown to contain populations of proliferative cells (Alié et al., 2011; Reitzel et al., 2016; Schnitzler et al., 2014). In our *Klf5a*- and *Klf5b*-knockdown experiments, the relative size of the tentacular median ridge was consistently reduced; therefore, we decided to perform EdU incorporation assays during mid-late embryogenesis to assess cell proliferation (Fig. S6). We observed reduced EdU incorporation in areas affected by the knockdown of *Klf5a* and *Klf5b*, including the tentacular median ridge and pharynx, suggesting that reduced cell proliferation rates are associated with the attenuation of zygotic *Klf5a* and *Klf5b* activity (Fig. S6J, K).

## DISCUSSION

Our expression analyses of *Klf5a* and *Klf5b* in *M. leidyi* shows that transcripts of both genes are maternally loaded and ubiquitously

distributed through gastrulation (Fig. 1B-E), corroborating previous RNA-seq results that detected abundant transcripts for both *Klf5a* and *Klf5b* during *M. leidyi* early-embryonic cleavage stages (Davidson et al., 2017). Knockdown of zygotic *Klf5a* and *Klf5b* expression did not appear to impact early embryonic development, because injected embryos underwent normal early cleavage and gastrulation. The zygotic expression of *Klf5a* and *Klf5b* displays localized spatiotemporal patterns in post-gastrulation embryos and transcripts because both *Klf5a* and *Klf5b* are expressed in the developing pharynx, gastrodermis, tentacle bulbs and apical organ (Fig. 1F-Q). These similar expression patterns could reflect functionally redundant roles (Lynch and Conery, 2000). By contrast, the expression of *KlfX* transcripts is restricted to late stages of development in a subset of apical organ epithelial cells (Fig. S1C, D). The *M. leidyi* *KlfX* gene sequence is highly divergent relative to other metazoan Klf genes (Presnell et al., 2015), suggestive of a *Mnemiopsis*-specific functional role for *KlfX*.

The Klf gene complement in *M. leidyi* is reduced compared with other non-bilaterian lineages (Presnell et al., 2015), a trend observed in other ctenophore gene families (Moroz et al., 2014; Ryan et al., 2013). Klf5-like genes are found in all metazoans (McCulloch and Koenig, 2020; Presnell et al., 2015). Among the non-bilaterian phyla, a *Klf5* ortholog in the cnidarian *Nematostella vectensis* genome was shown to be expressed in a cluster of cells associated with digestive filaments and the gastrodermis (Sebé-Pedrós et al., 2018a). In sponges, a *Klf5* ortholog was found to be expressed in stem cell-like archaeocytes in the marine sponge *Amphimedon queenslandica* (Sebé-Pedrós et al., 2018b) and in the digestive choanocytes and peptidocytes of the freshwater sponge *Spongilla lacustris* (Musser et al., 2019 preprint). In vertebrates, *Klf5* orthologs are required for the maintenance of intestinal crypt epithelia in the gut (Gao et al., 2015; Kuruvilla et al., 2015; McConnell et al., 2011; Nandan et al., 2015). Although less is known about *Klf5* orthologs from invertebrate bilaterians, *Klf5* is expressed in several cephalopod embryonic tissues, including yolk cells and the developing mouth (McCulloch and Koenig, 2020). In our previous phylogenetic study, it was unclear whether the few identified invertebrate sequences were either *Klf4* or *Klf5*, which share high sequence similarity (Presnell et al., 2015). One of these sequences, *Drosophila melanogaster dar1*, shares sequence similarity with human *KLF5* but has a functional role more similar to human *KLF4*, and was shown to play a role in regulation of gut proliferation (Wu et al., 2018b). Based on our expression analysis of *Klf5a* and *Klf5b* and the observed dysregulation of gastrodermal patterning in *Klf5a+Klf5b* knockdown embryos, our data suggest an evolutionarily conserved role for Klf5-like orthologs in the regulation and maintenance of gut epithelia among metazoans.

*M. leidyi* endodermal cell lineages stem from early-cleavage stage E and M oral macromeres, whereas ectodermal lineages originate from the aboral micromeres. Fate-mapping experiments show that the ectodermal micromeres contribute to the epidermis, ctene rows, tentacle epithelia and colloblasts, balancer cilia and the epithelial floor of the apical organ, whereas the endodermal macromeres give rise to the gastrodermis and associated endodermal canal system, muscle, tentacular median ridge and apical organ lithocytes (Henry and Martindale, 2001; Martindale and Henry, 1997a, 1999). Dysregulation of *Klf5a* and *Klf5b* showed consistent abnormal phenotypes associated with the development of the apical organ and tentacle bulbs. In the apical organ of *Klf5a*- and *Klf5b*-dysregulated embryos, the development of endodermally derived lithocytes was reduced or absent, whereas the ectodermally derived epithelial floor, balancer cilia and dome cilia appeared to be normal (Fig. 4A-G). Similarly, in the



developing tentacle bulb, abrogation of *Klf5a* and *Klf5b* activity resulted in the absence or reduction in size of the endodermally derived tentacular median ridge, which gives rise to the tentacle muscular core (Alié et al., 2011; Fig. 4H-N; Fig. S6L-N). Remaining tentacle tissue likely represents ectodermal contributions to tentacle epithelia and colloblasts. The development of other ectodermally derived structures, including the stomodeum and epidermal cells (Martindale and Henry, 1999), was unaffected (Fig. 4O-T). These results suggest that *Klf5a* and *Klf5b* play a functional role in the development and maintenance of endodermally derived tissues during *M. leidyi* embryogenesis.

With regard to the unique ectodermal expression domain of *Klf5b* (Fig. S1A,B), overall, no ectodermal or ctene row patterning phenotypes were observed in KLF-Cas9 embryos. In a few cases, ctene rows showed gross spatial disorganization, possibly reflecting a requirement for coordinated contact between ectoderm and underlying endoderm for precise ctene row alignment. For example, in phenotypically mild KLF-MO and KLF-Cas9 embryos, ctene row morphogenesis did not occur in quadrants in which endodermal tissue failed to contact ectodermal tissue (Fig. 3A,F,N). This result corroborates prior analyses indicating that ctene row development is at least partially regulated through inductive interactions between endodermal and ectodermal cell lineages (Fischer et al., 2014; Henry and Martindale, 2001, 2004; Martindale and Henry, 1997a). One possible explanation for the observed *Klf5b* expression pattern could be that *Klf5b* is expressed in developing light-producing photocytes derived from endodermal 2M macromeres that run subjacent to the ctene rows (Anctil, 1985; Fischer et al., 2014; Freeman and Reynolds, 1973; Martindale and Henry, 1999; Schnitzler et al., 2012). An EdU-positive ring of proliferative cells was situated around the ctene rows (Fig. S6C,G). These proliferative, *Klf5b*-positive cells may represent photocyte progenitor cells, because photocytes differentiate relatively early during development (Fischer et al., 2014). Notably, the initial development of differentiated polster cells/ctenes is specified by maternal factors, with additional ctenes generated post-embryonically. Therefore, zygotic *Klf5b* would not directly impact the specification of the initial ctenes during the stages observed in our study. An alternative explanation is that these *Klf5b*- and EdU-positive ectodermal cells represent progenitor cells that will give rise to new polster cells post-hatching and, thus, contribute to ctene row expansion.

In mammalian lineages, *Klf5* orthologs help maintain stem cell renewal and promote proliferation in the intestinal crypt and in pluripotent embryonic stem cells (Jiang et al., 2008; Kuruvilla et al., 2015; Nandan et al., 2015; Parisi et al., 2008, 2010). However, a recent study suggests that mammalian pluripotency factors are not necessarily conserved in all animals, and the ancestral metazoan stem cell toolkit primarily consisted of genes associated with the germline multipotency program (Alié et al., 2015; Juliano et al., 2010). Germline genes, including *Piwi*, *Bruno* and *Pl-10*, have been shown to be expressed in putative progenitor cell populations in the tentacle bulb, ctene rows and apical organ of adult *Pleurobrachia* (Alié et al., 2011). In *M. leidyi* cydippids, *Piwi*, *Vasa*, as well as Sox pluripotency factors are expressed in these same tissues, suggesting that progenitor cell populations in these tissues express both pluripotency factors and germline factors (Reitzel et al., 2016; Schnitzler et al., 2014). Our EdU staining recapitulates earlier work identifying zones of cell proliferation associated with the developing pharynx, gastrodermis, areas around the ctene rows and in the apical organ epithelial floor (Reitzel et al., 2016; Schnitzler et al., 2014; Fig. S6B-I). These areas of cell proliferation correlate with the

zygotic transcript expression domains, including the tentacular median ridge, of both *Klf5a* and *Klf5b* (Fig. 1; Fig. S6J).

Notably, sponge orthologs to *Klf5*, *Piwi*, *Bruno* and *Pl-10* are expressed in archaeocytes and choanocytes variably recognized as sponge equivalents to totipotent, pluripotent and/or multipotent stem cells (Alié et al., 2015; Musser et al., 2019 preprint; Nakanishi et al., 2014; Sebé-Pedrós et al., 2018b; Sogabe et al., 2019). Although we were unable to perform quantitative analyses, our qualitative assessments showed a diminution/loss of EdU-positive cells in the tentacular median ridge and apical organ in *Klf5a+Klf5b*-knockdown embryos (Fig. S6K). One interpretation of our results is that *Klf5a* and *Klf5b* are expressed in proliferative cells and play a functional role in the maintenance of multipotent endodermal progenitor cell populations.

To resolve whether *Klf5a*- or *Klf5b*-expressing cells are both proliferative and multipotent will require additional experimentation. Future experiments involving the knockdown of pluripotency and germline determination genes, such as *Piwi* and *Vasa*, along with EdU assays may reveal further aspects of cellular proliferation and specification associated with Klf activity. Alternatively, the observed phenotypes may result from proliferation-independent mechanisms establishing terminal cell identity. For example, *Klf5a* and *Klf5b* may regulate the terminal specification of lithocyte and tentacle muscle cell types. Based on this work, although the explicit regulatory role of *Klf5a* and *Klf5b* remains unclear, our results show that *Klf5a* and *Klf5b* are functionally associated with the formation, developmental patterning and maintenance of endodermally derived structures in *M. leidyi*, including the gastrodermis, tentacular median ridge, tentacle muscle and apical organ lithocytes. This functional activity may occur through the maintenance of multipotent progenitor cell proliferation and may represent a conserved ancestral function for this transcription factor gene family in the animal stem lineage. Overall, our results begin to lay the groundwork for assessing gene functions that are essential for the embryonic development of *M. leidyi* and, thus, inform developmental mechanisms unique to Ctenophora for the specification of terminally differentiated tissue and cell types (e.g. lithocytes).

In this study, we report the first use of CRISPR/Cas9 mutagenesis to investigate gene function in a species of ctenophore. We describe techniques that are cost effective and can easily be used to assess phenotypes and validate Cas9 activity (e.g. vital dye labeling and Sanger sequencing). This foundational work shows that CRISPR/Cas9 is an effective method for evaluating developmental phenotypes from single or combinatorial gene function loss in G0 ctenophore embryos. Future studies can refine our protocol to generate more-efficient CRISPR/Cas9 mutagenesis by choosing different targets within loci (e.g. the transcriptional start site) and by increasing or modifying Cas9 exonuclease activity. Techniques have recently been developed that improve Cas9 editing, resulting in high percentages (>80%) of indel mutations (Hoshijima et al., 2019; Wu et al., 2018a). Although cell-autonomous phenotypes can be detected in G0 Cas9-injected embryos, which is useful for generating hypotheses regarding gene function, the characterization of stable and heritable non-lethal mutations (i.e. in F1 embryos) would be even better. *M. leidyi* are self-fertile hermaphrodites that could be leveraged to enable rapid creation of stable lines useful for characterization of mutations generated via CRISPR/Cas9. Along with recent RNA-seq data highlighting candidate genes associated with zygotic gene activation and patterning of specific cell types in ctenophores (Babonis et al., 2018; Davidson et al., 2017; Sebé-Pedrós et al., 2018b), CRISPR/Cas9 mutagenesis in *M. leidyi* (and

potentially other ctenophore species) will provide much needed insight into the genetic mechanisms underlying unique facets of ctenophore biology (Bessho-Uehara et al., 2020; Jokura et al., 2019; Yamada et al., 2010), furthering our understanding of early metazoan evolution.

## MATERIALS AND METHODS

### Cloning and *in situ* hybridization

RNA was extracted using Trizol (Thermo Fisher Scientific) from *Mnemiopsis* embryos collected at different developmental stages and used to generate cDNA libraries (SMARTer kit, Clontech). The coding sequences of *Klf5a*, *Klf5b* and *KlfX* were amplified from cDNA (Table 1) and cloned into a pGEM-T Easy vector (Promega). The cloned fragments were used as templates for *in vitro* transcription (MEGAscript, Ambion) of antisense digoxigenin-labeled (Digoxigenin-11-UTP, Roche) riboprobes.

*In situ* hybridization (ISH) followed the methodology of Pang and Martindale (2008). Riboprobes were used at a final concentration of ~0.5 ng/μl and hybridized with embryos for 24 h. After color development, nuclei were labeled with either DAPI (Molecular Probes) or Hoechst 33342 (Molecular Probes) in 1× PBS. Embryos were immediately imaged or stored at -20°C in 70% glycerol in 1× PBS. Images were acquired using a Zeiss Axio Imager.Z2, Zeiss AxioCam MRm Rev3 camera and Zeiss Zen Blue software. Fluorescent Z-stacks were deconvolved, post-processed for brightness and contrast and assembled in Adobe Photoshop. Monochrome brightfield images were inverted, pseudo colored and overlaid onto fluorescent images of labeled nuclei.

### EdU labeling

A Click-iT® EdU Alexa Fluor® 647 Imaging Kit (Thermo Fisher Scientific) was used for identification of proliferating cells. Embryos were collected at different developmental stages and pulse incubated for 25 min with 100 μM EdU in a solution of a 1:1 volumetric ratio of artificial seawater (FSW) to 6.5% MgCl<sub>2</sub> (dissolved in dH<sub>2</sub>O) at room temperature. The EdU solution was washed out and embryos were either fixed immediately or allowed to continue to develop during a 24-h chase and subsequently fixed. Embryos were fixed with 4% PFA in FSW for 30 min at room temperature, washed with 3% BSA in 1× PBS and then incubated with 0.5% Triton X-100 in 1× PBS for 20 min at room temperature. Fixed embryos were washed with 3% BSA in 1× PBS and stored at 4°C until used for EdU detection as per the manufacturer's protocol. Embryos were subsequently washed with 1× PBS and mounted on glass microscope slides. Images were acquired using a Zeiss Axio Imager.Z2, Zeiss AxioCam MRm Rev3 camera and Zeiss Zen Blue software. Fluorescent Z-stacks were deconvolved, post-processed for brightness and contrast, and assembled in Adobe Photoshop or FIJI (Schindelin et al., 2012).

### Preparation and microinjection of embryos

Microinjection needles were pulled with a Brown micropipette puller (P-1000, Sutter Instrument Company) using filamented aluminosilicate glass capillaries (AF100-64-10, Sutter Instrument Company). Pulled capillary needles were beveled using a microelectrode beveler (BV-10, Sutter Instrument Company). Beveling creates a consistent microinjection needle with uniform tip characteristics optimized for egg penetration and substantially reduces embryo mortality. Beveled capillary needles were loaded via backfilling with injection cocktails mixed with fluorescently conjugated dextran (Invitrogen) for rapid assessment of injection success and subsequent lineage tracing. Loaded capillary needles were mounted to a Xeneworks microinjection system (Sutter Instrument Company) paired to a Zeiss Discovery V8 epifluorescence stereomicroscope.

Microinjection dishes were designed to aid stabilizing and positioning of embryos during injections. In a 30 mm or 60 mm Petri dish, a glass microscope slide was placed at a 30-45° angle. Molten 2% agarose (dissolved in 1:1 volume FSW:dH<sub>2</sub>O) was slowly poured into the dish until the agarose meniscus reached the underside of the angled glass slide. Once the agarose solidified, the glass slide was removed, creating a molded ramp impression terminating in a 90° trough. For short-term storage of agarose molds between microinjection sessions, we flooded dishes with 1×

penicillin/streptomycin (Sigma-Aldrich):FSW (PS:FSW), sealed and stored at 4°C.

Laboratory cultures of adult *M. leidyi* on a ~12 h/12 h light:dark cycle were spawned ~4 h post-darkness (hpd). At ~3.5 hpd, individual adult *M. leidyi* were placed into 8-inch glass bowls (Carolina Biological Supply) and screened for mature sperm and eggs. Freshly fertilized eggs were collected by pipette and passed sequentially through a 500 μm and then a 400 μm cell strainer (pluriSelect Life Science) to remove excess mucus and egg jelly. Embryos were then washed with PS:FSW. Ctenophore vitelline membranes are resistant to penetration from microinjection needles and must be removed. Additionally, the highly viscous inner egg jelly, which will clog the injection needle, should be removed from the egg surface. In gelatin-coated dishes filled with PS:FSW, we used acid-sharpened tungsten needles to remove both the vitelline membranes and underlying egg jelly. A 5× gelatin stock (0.5% Knox Original Unflavored Gelatin dissolved in dH<sub>2</sub>O, with formalin added to a final concentration of 0.19%) was diluted to 1× with dH<sub>2</sub>O, poured into dishes, swirled and then discarded. Once the gelatin dried, the dishes were rinsed several times with dH<sub>2</sub>O. Applying a gelatin coating helps prevent devitellinized embryos from adhering to plastic, glass and metal surfaces. We applied a gelatin coat to glass and plastic dishes, transfer pipettes, and dissecting needles. Once the vitelline membranes and egg jelly were removed, embryos were then carefully transferred to an injection dish and positioned along the agarose trough for microinjection. After injections, embryos were kept at room temperature in gelatin-coated dishes until reaching the desired development stage for further analyses.

### Morpholino oligonucleotides

sbMOs (Gene Tools) were designed for both *Klf5a* (*ML00922a*) and *Klf5b* (*ML25776a*). *Klf5a* sbMO1 and sbMO2 targeted the intron 2-exon 3 and intron 3-exon 4 boundaries, respectively. *Klf5b* sbMO1 and sbMO2 targeted the exon 6-intron 6 and exon 7-intron 7 boundaries, respectively. A standard control MO was used as a negative control. Sequences of sbMOs are listed in Table 1. Stock solutions of sbMO in dH<sub>2</sub>O were stored at room temperature. sbMO injection cocktail solutions consisted of a final sbMO concentration of ~333 nM and ~0.5 mg/ml fluorescent dextran (rhodamine or Alexa-Fluor 488, 10,000 molecular weight; Invitrogen) in 35% glycerol. After phenotypic analyses via vital-dye staining and microscopy, RNA was extracted from individual embryos (Arcturus PicoPure, Thermo Fisher Scientific) and cDNA was prepared. Gene-specific primers were used on cDNA (OneTaq One-Step RT-PCR; New England Biolabs) to evaluate aberrant transcript splicing via gel electrophoresis. A total of 45 embryos were injected with a *Klf5a+Klf5b* double-gene knockdown sbMO cocktail and used for all downstream analyses.

### CRISPR/Cas9 mutagenesis

We followed a cloning-free method to generate sgRNAs (Kistler et al., 2015; Varshney et al., 2015). PCR-amplified templates were generated by annealing a 20-nucleotide universal tracrRNA oligo to a sgRNA-specific oligo that consisted of a T7 promoter, followed by the sgRNA target sequence and a complementary sequence to the tracrRNA oligo (Table 1). These templates were then *in vitro* transcribed (MEGAscript, Ambion) to generate sgRNAs. The CasOT program (Xiao et al., 2014) and *M. leidyi* reference genome (Moreland et al., 2014, 2020) were used to identify sgRNA target sites for *Klf5a* (*ML00922a*), *Klf5b* (*ML25776a*), and *KlfX* (*ML20061a*). We selected sgRNAs that had no fewer than four mismatches to alternative genomic sites to minimize potential OTS activity (Tables 1 and 2). Recombinant Cas9 protein (PNA Bio) and sgRNAs were injected at concentrations of 400 ng/μl of Cas9 protein and 100 ng/μl for each sgRNA. A total of 17 embryos from *Klf5a+Klf5b* double-gene knockout sgRNA/Cas9 cocktail injections were live imaged and processed for downstream analyses. After phenotypic analysis, genomic DNA was extracted from individual embryos (QIAamp DNA Micro, Qiagen) and each sgRNA target site was amplified and Sanger sequenced. The ICE analysis tool (Hsiau et al., 2019 preprint) was used to determine Cas9 efficiency for each sgRNA. ICE analysis gives two scores: an ICE score, which reflects the percentage of indels found, and a KO score, which reflects the percentage of indels that produce a frameshift mutation. We obtained ICE/sequencing information and analyzed OTSs from all 17 embryos for *Klf5b* cut sites and 14 of the 17

embryos for *Klf5a* cut sites. We were unable to obtain sequence information at the *Klf5a* locus for three of the embryos. Additional single-gene injection analyses, either *Klf5a* or *Klf5b*, were performed on five embryos per gene.

### Phenotypic analysis through vital dye staining

Control, sbMO and Cas9-injected embryos at 20–24 hpf were incubated in FSW containing a final concentration of 100 nM MitoTracker (Deep Red FM, Molecular Probes), 100 nM LysoTracker (Red DND-99, Molecular Probes) and 10 ng/μl Hoechst 33342 for 1 h at room temperature. The live embryos were then placed on glass slides in a drop of FSW and relaxed with a drop of 6.5% MgCl<sub>2</sub> (in dH<sub>2</sub>O) on a coverslip positioned with clay feet for imaging. Differential interference contrast (DIC) and fluorescent images were acquired using a Zeiss Axio Imager.Z2, Zeiss AxioCam MRm Rev3 camera and Zeiss Zen Blue software. Fluorescent Z-stacks were deconvolved, post-processed for brightness and contrast, and assembled in Adobe Photoshop.

### Epidermal nuclei counts

A subset of live images from wild-type, KLF-MO and KLF-Cas9 embryos were used (see previous section) to quantitate epidermal nuclei. Individual Z-sections from Hoechst channels were focused on the outer epidermal layer for each embryo oriented along the TA. A 100 μm<sup>2</sup> region of interest (roi) was positioned medially and orally to the ctene rows. Nuclei within the roi were manually counted. Nuclei counts were quantified and plotted using R (<http://shiny.chemgrid.org/boxplotr/>).

### Statistical analysis

The Student's two-tailed unpaired *t*-test was used to calculate the *P*-values for comparisons between two different groups. A confidence interval of 95% was used to determine statistical significance. Box and whisker plots were generated with R (<http://shiny.chemgrid.org/boxplotr/>). Box limits indicate the 25th and 75th percentiles and the whiskers extend 1.5× the interquartile range from the 25th and 75th percentiles. Centerlines show the medians and crosses represent the sample means. Data points outside the ends of the whiskers are outliers.

### Acknowledgements

We thank Ricardo Cepeda for additional animal support, Julia Dallman for logistical support and anonymous reviewers for their time and generous feedback.

### Competing interests

The authors declare no competing or financial interests.

### Author contributions

Conceptualization: W.E.B.; Methodology: J.S.P., W.E.B.; Validation: W.E.B.; Formal analysis: J.S.P., W.E.B.; Investigation: J.S.P., W.E.B.; Resources: W.E.B.; Data curation: J.S.P., W.E.B.; Writing - original draft: J.S.P., W.E.B.; Writing - review & editing: J.S.P., W.E.B.; Visualization: J.S.P., W.E.B.; Supervision: W.E.B.; Project administration: W.E.B.; Funding acquisition: W.E.B.

### Funding

This work was supported, in part, by startup funds from the University of Miami College of Arts and Sciences to W.E.B. J.S.P. was supported by the University of Miami College of Arts and Sciences.

### References

Alié, A., Leclère, L., Jager, M., Dayraud, C., Chang, P., Le Guyader, H., Quéinnec, E. and Manuel, M. (2011). Somatic stem cells express *Piwi* and *Vasa* genes in an adult ctenophore: ancient association of "germline genes" with stemness. *Dev. Biol.* **350**, 183–197. doi:10.1016/j.ydbio.2010.10.019

Alié, A., Hayashi, T., Sugimura, I., Manuel, M., Sugano, W., Mano, A., Satoh, N., Agata, K. and Funayama, N. (2015). The ancestral gene repertoire of animal stem cells. *Proc. Natl. Acad. Sci. USA* **112**, E7093–E7100. doi:10.1073/pnas.1514789112

Anctil, M. (1985). Ultrastructure of the luminescent system of the ctenophore *Mnemiopsis leidyi*. *Cell Tissue Res.* **242**, 333–340. doi:10.1007/BF00214545

Babonis, L. S., DeBiasse, M. B., Francis, W. R., Christianson, L. M., Moss, A. G., Haddock, S. H. D., Martindale, M. Q. and Ryan, J. F. (2018). Integrating embryonic development and evolutionary history to characterize tentacle-specific

cell types in a ctenophore. *Mol. Biol. Evol.* **35**, 2940–2956. doi:10.1093/molbev/msy171

Bessho-Uehara, M., Huang, W., Patry, W. L., Browne, W. E., Weng, J.-K. and Haddock, S. H. D. (2020). Evidence for de novo biosynthesis of the luminous substrate Coelenterazine in Ctenophores. *iScience* **23**, 101859. doi:10.1016/j.isci.2020.101859

Bialkowska, A. B., Yang, V. W. and Mallipattu, S. K. (2017). Krüppel-like factors in mammalian stem cells and development. *Development* **144**, 737–754. doi:10.1242/dev.145441

Blakeley, P., Fogarty, N. M. E., Del Valle, I., Wamaitha, S. E., Hu, T. X., Elder, K., Snell, P., Christie, L., Robson, P. and Niakan, K. K. (2015). Defining the three cell lineages of the human blastocyst by single-cell RNA-seq. *Development* **142**, 3613. doi:10.1242/dev.131235

Davidson, P. L., Koch, B. J., Schnitzler, C. E., Henry, J. Q., Martindale, M. Q., Baxevasis, A. D. and Browne, W. E. (2017). The maternal-zygotic transition and zygotic activation of the *Mnemiopsis leidyi* genome occurs within the first three cleavage cycles. *Mol. Reprod. Dev.* **84**, 1218–1229. doi:10.1002/mrd.22926

De Graeve, F., Smaldone, S., Laub, F., Mlodzik, M., Bhat, M. and Ramirez, F. (2003). Identification of the *Drosophila* progenitor of mammalian Krüppel-like factors 6 and 7 and a determinant of fly development. *Gene* **314**, 55–62. doi:10.1016/S0378-1119(03)00720-0

DuBuc, T. Q., Schnitzler, C. E., Chrysostomou, E., McMahon, E. T., Febrimarsa, F., Gahan, J. M., Buggie, T., Gornik, S. G., Hanley, S., Barreira, S. N. et al. (2020). Transcription factor AP2 controls cnidarian germ cell induction. *Science* **367**, 757–762. doi:10.1126/science.aay6782

Dunn, C. W., Hejnal, A., Matus, D. Q., Pang, K., Browne, W. E., Smith, S. A., Seaver, E., Rouse, G. W., Obst, M., Edgecombe, G. D. et al. (2008). Broad phylogenomic sampling improves resolution of the animal tree of life. *Nature* **452**, 745–749. doi:10.1038/nature06614

Fischer, A. H., Pang, K., Henry, J. Q. and Martindale, M. Q. (2014). A cleavage clock regulates features of lineage-specific differentiation in the development of a basal branching metazoan, the ctenophore *Mnemiopsis leidyi*. *Evodevo* **5**, 4. doi:10.1186/2041-9139-5-4

Freeman, G. (1976). The effects of altering the position of cleavage planes on the process of localization of developmental potential in ctenophores. *Dev. Biol.* **51**, 332–337. doi:10.1016/0012-1606(76)90148-2

Freeman, G. and Reynolds, G. T. (1973). The development of bioluminescence in the ctenophore *Mnemiopsis leidyi*. *Dev. Biol.* **31**, 61–100. doi:10.1016/0012-1606(73)90321-7

Gao, Y., Cao, Q., Lu, L., Zhang, X., Zhang, Z., Dong, X., Jia, W. and Cao, Y. (2015). Kruppel-like factor family genes are expressed during *Xenopus* embryogenesis and involved in germ layer formation and body axis patterning. *Dev. Dyn.* **244**, 1328–1346. doi:10.1002/dvdy.24310

Hejnal, A., Obst, M., Stamatakis, A., Ott, M., Rouse, G. W., Edgecombe, G. D., Martinez, P., Baguñà, J., Bailly, X., Jondelius, U. et al. (2009). Assessing the root of bilaterian animals with scalable phylogenomic methods. *Proc. R. Soc. B Biol. Sci.* **276**, 4261–4270. doi:10.1098/rspb.2009.0896

Hemrich, G., Khalturin, K., Boehm, A.-M., Puchert, M., Anton-Erxleben, F., Wittlieb, J., Klostermeier, U. C., Rosenstiel, P., Oberg, H.-H., Domazet-Lošo, T. et al. (2012). Molecular signatures of the three stem cell lineages in hydra and the emergence of stem cell function at the base of multicellularity. *Mol. Biol. Evol.* **29**, 3267–3280. doi:10.1093/molbev/mss134

Henry, J. Q. and Martindale, M. Q. (2001). Multiple inductive signals are involved in the development of the ctenophore *Mnemiopsis leidyi*. *Dev. Biol.* **238**, 40–46. doi:10.1006/dbio.2001.0401

Henry, J. Q. and Martindale, M. Q. (2004). Inductive interactions and embryonic equivalence groups in a basal metazoan, the ctenophore *Mnemiopsis leidyi*. *Evol. Dev.* **6**, 17–24. doi:10.1111/j.1525-142X.2004.04001.x

Horridge, G. A. (1964a). Presumed photoreceptive cilia in a ctenophore. *J. Cell Sci.* **s3-105**, 311–317. doi:10.1242/jcs.s3-105.71.311

Horridge, G. A. (1964b). The giant mitochondria of ctenophore comb-plates. *J. Cell Sci.* **s3-105**, 301–310. doi:10.1242/jcs.s3-105.71.301

Hoshijima, K., Juryneć, M. J., Shaw, D. K., Jacobi, A. M., Behlke, M. A. and Grunwald, D. J. (2019). Highly efficient CRISPR-Cas9-based methods for generating deletion mutations and F0 embryos that lack gene function in zebrafish. *Dev. Cell* **51**, 645–657.e4. doi:10.1016/j.devcel.2019.10.004

Hsiau, T., Conant, D., Rossi, N., Maures, T., Waite, K., Yang, J., Joshi, S., Kelso, R., Holden, K., Enzmann, B. L. et al. (2019). Inference of CRISPR edits from sanger trace data. *bioRxiv* doi:10.1101/251082

Illesley, M. D., Gillinder, K. R., Magor, G. W., Huang, S., Bailey, T. L., Crossley, M. and Perkins, A. C. (2017). Krüppel-like factors compete for promoters and enhancers to fine-tune transcription. *Nucleic Acids Res.* **45**, 6572–6588. doi:10.1093/nar/gkx441

Jager, M., Quéinnec, E., Chiori, R., Le Guyader, H. and Manuel, M. (2008). Insights into the early evolution of SOX genes from expression analyses in a ctenophore. *J. Exp. Zool. B Mol. Dev. Evol.* **310B**, 650–667. doi:10.1002/jez.b.21244

Jiang, J., Chan, Y.-S., Loh, Y.-H., Cai, J., Tong, G.-Q., Lim, C.-A., Robson, P., Zhong, S. and Ng, H.-H. (2008). A core Klf circuitry regulates self-renewal of embryonic stem cells. *Nat. Cell Biol.* **10**, 353–360. doi:10.1038/ncb1698

- Jokura, K. and Inaba, K.** (2020). Structural diversity and distribution of cilia in the apical sense organ of the ctenophore *Bolinopsis mikado*. *Cytoskeleton* **77**, 442-455. doi:10.1002/cm.21640
- Jokura, K., Shibata, D., Yamaguchi, K., Shiba, K., Makino, Y., Shigenobu, S. and Inaba, K.** (2019). CTENO64 is required for coordinated paddling of ciliary comb plate in ctenophores. *Curr. Biol.* **29**, 3510-3516.e4. doi:10.1016/j.cub.2019.08.059
- Juliano, C. E., Swartz, S. Z. and Wessel, G. M.** (2010). A conserved germline multipotency program. *Development* **137**, 4113-4126. doi:10.1242/dev.047969
- Kapli, P. and Telford, M. J.** (2020). Topology-dependent asymmetry in systematic errors affects phylogenetic placement of Ctenophora and Xenacoelomorpha. *Sci. Adv.* **6**, eabc5162. doi:10.1126/sciadv.abc5162
- Kistler, K. E., Voshall, L. B. and Matthews, B. J.** (2015). Genome engineering with CRISPR-Cas9 in the mosquito *Aedes aegypti*. *Cell Rep.* **11**, 51-60. doi:10.1016/j.celrep.2015.03.009
- Kult, S., Olender, T., Osterwalder, M., Markman, S., Leshkowitz, D., Krief, S., Blecher-Gonen, R., Ben-Moshe, S., Farack, L., Keren-Shaul, H. et al.** (2021). Bi-fated tendon-to-bone attachment cells are regulated by shared enhancers and KLF transcription factors. *eLife* **10**, e55361. doi:10.7554/eLife.55361
- Kuruvilla, J. G., Ghaleb, A. M., Bialkowska, A. B., Nandan, M. O. and Yang, V. W.** (2015). Role of Krüppel-like factor 5 in the maintenance of the stem cell niche in the intestinal crypt. *Stem Cell Transl. Invest.* **2**, e839.
- Levy, S., Elek, A., Grau-Bové, X., Menéndez-Bravo, S., Iglesias, M., Taney, A., Mass, T. and Sebé-Pedrós, A.** (2021). A stony coral cell atlas illuminates the molecular and cellular basis of coral symbiosis, calcification, and immunity. *Cell* **184**, 2973-2987.E18. doi:10.1016/j.cell.2021.04.005
- Li, Y., Shen, X.-X., Evans, B., Dunn, C. W. and Rokas, A.** (2021). Rooting the animal tree of life. *Mol. Biol. Evol.* msab170. doi:10.1093/molbev/msab170
- Lynch, M. and Conery, J. S.** (2000). The evolutionary fate and consequences of duplicate genes. *Science* **290**, 1151-1155. doi:10.1126/science.290.5494.1151
- Martindale, M. Q. and Henry, J. Q.** (1997a). Reassessing embryogenesis in the Ctenophora: the inductive role of e1 micromeres in organizing ctenophore formation in the 'mosaic' embryo. *Mnemiopsis leidyi*. *Development* **124**, 1999-2006. doi:10.1242/dev.124.10.1999
- Martindale, M. Q. and Henry, J. Q.** (1997b). Experimental analysis of tentacle formation in the Ctenophore *Mnemiopsis leidyi*. *Biol. Bull.* **193**, 245-247. doi:10.1086/BBLV193n2p245
- Martindale, M. Q. and Henry, J. Q.** (1999). Intracellular fate mapping in a basal metazoan, the ctenophore *Mnemiopsis leidyi*, reveals the origins of mesoderm and the existence of indeterminate cell lineages. *Dev. Biol.* **214**, 243-257. doi:10.1006/dbio.1999.9427
- Martindale, M. Q. and Henry, J. Q.** (2015). Ctenophora. In *Evolutionary Developmental Biology of Invertebrates 1: Introduction, Non-Bilateria, Acoelomorpha, Xenoturbellida, Chaetognatha* (ed. A. Wanninger), pp. 179-201. Vienna: Springer Vienna.
- McConnell, B. B. and Yang, V. W.** (2010). Mammalian Krüppel-like factors in health and diseases. *Physiol. Rev.* **90**, 1337-1381. doi:10.1152/physrev.00058.2009
- McConnell, B. B., Kim, S. S., Yu, K., Ghaleb, A. M., Takeda, N., Manabe, I., Nusrat, A., Nagai, R. and Yang, V. W.** (2011). Krüppel-like factor 5 is important for maintenance of crypt architecture and barrier function in mouse intestine. *Gastroenterology* **141**, 1302-1313.e6. doi:10.1053/j.gastro.2011.06.086
- McCulloch, K. J. and Koening, K. M.** (2020). Krüppel-like factor/specificity protein evolution in the Spiralia and the implications for cephalopod visual system novelties. *Proc. R. Soc. B Biol. Sci.* **287**, 20202055. doi:10.1098/rspb.2020.2055
- Moore, D. L., Blackmore, M. G., Hu, Y., Kaestner, K. H., Bixby, J. L., Lemmon, V. P. and Goldberg, J. L.** (2009). KLF family members regulate intrinsic axon regeneration ability. *Science* **326**, 298-301. doi:10.1126/science.1175737
- Moreland, R. T., Nguyen, A.-D., Ryan, J. F., Schnitzler, C. E., Koch, B. J., Siewert, K., Wolfsberg, T. G. and Baxeavanis, A. D.** (2014). A customized Web portal for the genome of the ctenophore *Mnemiopsis leidyi*. *BMC Genomics* **15**, 316. doi:10.1186/1471-2164-15-316
- Moreland, R. T., Nguyen, A.-D., Ryan, J. F. and Baxeavanis, A. D.** (2020). The *Mnemiopsis* genome project portal: integrating new gene expression resources and improving data visualization. *Database* **2020**, baaa029. doi:10.1093/database/baaa029
- Moroz, L. L., Kocot, K. M., Citarella, M. R., Dosung, S., Norekian, T. P., Povolotskaya, I. S., Grigorenko, A. P., Dailey, C., Berezikov, E., Buckley, K. M. et al.** (2014). The ctenophore genome and the evolutionary origins of neural systems. *Nature* **510**, 109-114. doi:10.1038/nature13400
- Musser, J. M., Schippers, K. J., Nickel, M., Mizzon, G., Kohn, A. B., Pape, C., Hammel, J. U., Wolf, F., Liang, C., Hernández-Plaza, A. et al.** (2019). Profiling cellular diversity in sponges informs animal cell type and nervous system evolution. *bioRxiv* doi:10.1101/758276
- Nagai, R., Friedman, S. L. and Kasuga, M.** (eds.). (2009). *The Biology of Krüppel-like Factors*. Tokyo: Springer.
- Nakanishi, N., Sogabe, S. and Degnan, B. M.** (2014). Evolutionary origin of gastrulation: insights from sponge development. *BMC Biol.* **12**, 26. doi:10.1186/1741-7007-12-26
- Nandan, M. O., Ghaleb, A. M., Bialkowska, A. B. and Yang, V. W.** (2015). Krüppel-like factor 5 is essential for proliferation and survival of mouse intestinal epithelial stem cells. *Stem Cell Res.* **14**, 10-19. doi:10.1016/j.scr.2014.10.008
- Oishi, Y. and Manabe, I.** (2018). Krüppel-like factors in metabolic homeostasis and cardiometabolic disease. *Front. Cardiovasc. Med.* **5**, 69. doi:10.3389/fcvm.2018.00069
- Pang, K. and Martindale, M. Q.** (2008). Ctenophore whole-mount in situ hybridization. *Cold Spring Harb. Protoc.* **2008**, pdb.prot5087. doi:10.1101/pdb.prot5087
- Parisi, S., Passaro, F., Aloia, L., Manabe, I., Nagai, R., Pastore, L. and Russo, T.** (2008). Klf5 is involved in self-renewal of mouse embryonic stem cells. *J. Cell Sci.* **121**, 2629-2634. doi:10.1242/jcs.027599
- Parisi, S., Cozzuto, L., Tarantino, C., Passaro, F., Ciriello, S., Aloia, L., Antonini, D., De Simone, V., Pastore, L. and Russo, T.** (2010). Direct targets of Klf5 transcription factor contribute to the maintenance of mouse embryonic stem cell undifferentiated state. *BMC Biol.* **8**, 128. doi:10.1186/1741-7007-8-128
- Pearson, R., Fleetwood, J., Eaton, S., Crossley, M. and Bao, S.** (2008). Krüppel-like transcription factors: a functional family. *Int. J. Biochem. Cell Biol.* **40**, 1996-2001. doi:10.1016/j.biocel.2007.07.018
- Presnell, J. S., Schnitzler, C. E. and Browne, W. E.** (2015). KLF/SP transcription factor family evolution: expansion, diversification, and innovation in eukaryotes. *Genome Biol. Evol.* **7**, 2289-2309. doi:10.1093/gbe/evv141
- Presnell, J. S., Vandepas, L. E., Warren, K. J., Swalla, B. J., Amemiya, C. T. and Browne, W. E.** (2016). The presence of a functionally tripartite through-gut in Ctenophora has implications for metazoan character trait evolution. *Curr. Biol.* **26**, 2814-2820. doi:10.1016/j.cub.2016.08.019
- Reitzel, A. M., Pang, K. and Martindale, M. Q.** (2016). Developmental expression of "germline"- and "sex determination"-related genes in the ctenophore *Mnemiopsis leidyi*. *Evodevo* **7**, 17. doi:10.1186/s13227-016-0051-9
- Ryan, J. F., Pang, K., Schnitzler, C. E., Nguyen, A.-D., Moreland, R. T., Simmons, D. K., Koch, B. J., Francis, W. R., Haviak, P., NISC Comparative Sequencing Program et al.** (2013). The genome of the ctenophore *Mnemiopsis leidyi* and its implications for cell type evolution. *Science* **342**, 1242592. doi:10.1126/science.1242592
- Salinas-Saavedra, M. and Martindale, M. Q.** (2020). Par protein localization during the early development of *Mnemiopsis leidyi* suggests different modes of epithelial organization in the metazoa. *eLife* **9**, e54927. doi:10.7554/eLife.54927
- Schindelin, J., Arganda-Carreeras, I., Frise, E., Kaynig, V., Longair, M., Pietzsch, T., Preibisch, S., Rueden, C., Saalfeld, S., Schmid, B. et al.** (2012). Fiji: an open-source platform for biological-image analysis. *Nat. Methods* **9**, 676-682. doi:10.1038/nmeth.2019
- Schnitzler, C. E., Pang, K., Powers, M. L., Reitzel, A. M., Ryan, J. F., Simmons, D., Tada, T., Park, M., Gupta, J., Brooks, S. Y. et al.** (2012). Genomic organization, evolution, and expression of photoprotein and opsin genes in *Mnemiopsis leidyi*: a new view of ctenophore photocytes. *BMC Biol.* **10**, 107. doi:10.1186/1741-7007-10-107
- Schnitzler, C. E., Simmons, D. K., Pang, K., Martindale, M. Q. and Baxeavanis, A. D.** (2014). Expression of multiple Sox genes through embryonic development in the ctenophore *Mnemiopsis leidyi* is spatially restricted to zones of cell proliferation. *Evodevo* **5**, 15. doi:10.1186/2041-9139-5-15
- Sebé-Pedrós, A., Saudemont, B., Chomsky, E., Plessier, F., Mailhé, M.-P., Renno, J., Loe-Mie, Y., Lifshitz, A., Mukamel, Z., Schmutz, S. et al.** (2018a). Cnidarian cell type diversity and regulation revealed by whole-organism single-cell RNA-seq. *Cell* **173**, 1520-1534.e20. doi:10.1016/j.cell.2018.05.019
- Sebé-Pedrós, A., Chomsky, E., Pang, K., Lara-Astiaso, D., Gaiti, F., Mukamel, Z., Amit, I., Hejnal, A., Degnan, B. M. and Tanay, A.** (2018b). Early metazoan cell type diversity and the evolution of multicellular gene regulation. *Nat. Ecol. Evol.* **2**, 1176-1188. doi:10.1038/s41559-018-0575-6
- Shen, X.-X., Hittinger, C. T. and Rokas, A.** (2017). Contentious relationships in phylogenomic studies can be driven by a handful of genes. *Nat. Ecol. Evol.* **1**, 0126. doi:10.1038/s41559-017-0126
- Siebert, S., Farrell, J. A., Cazet, J. F., Abeykoon, Y., Primack, A. S., Schnitzler, C. E. and Juliano, C. E.** (2019). Stem cell differentiation trajectories in Hydra resolved at single-cell resolution. *Science* **365**, eaav9314. doi:10.1126/science.aav9314
- Sogabe, S., Hatteberg, W. L., Kocot, K. M., Say, T. E., Stoupin, D., Roper, K. E., Fernandez-Valverde, S. L., Degnan, S. M. and Degnan, B. M.** (2019). Pluripotency and the origin of animal multicellularity. *Nature* **570**, 519-522. doi:10.1038/s41586-019-1290-4
- Sweet, D. R., Fan, L., Hsieh, P. N. and Jain, M. K.** (2018). Krüppel-like factors in vascular inflammation: mechanistic insights and therapeutic potential. *Front. Cardiovasc. Med.* **5**, 6. doi:10.3389/fcvm.2018.00006
- Tamm, S. L.** (1973). Mechanisms of ciliary co-ordination in ctenophores. *J. Exp. Biol.* **59**, 231-245. doi:10.1242/jeb.59.1.231
- Tamm, S. L.** (2012). Patterns of comb row development in young and adult stages of the ctenophores *Mnemiopsis leidyi* and *Pleurobrachia pileus*. *J. Morphol.* **273**, 1050-1063. doi:10.1002/jmor.20043
- Tamm, S. L.** (2014). Formation of the statolith in the ctenophore *Mnemiopsis leidyi*. *Biol. Bull.* **227**, 7-18. doi:10.1086/BBLV227n1p7

- Tarashansky, A. J., Musser, J. M., Khariton, M., Li, P., Arendt, D., Quake, S. R. and Wang, B.** (2021). Mapping single-cell atlases throughout Metazoa unravels cell type evolution. *eLife* **10**, e66747. doi:10.7554/eLife.66747
- Varshney, G. K., Pei, W., LaFave, M. C., Idol, J., Xu, L., Gallardo, V., Carrington, B., Bishop, K., Jones, M. P., Li, M. et al.** (2015). High-throughput gene targeting and phenotyping in zebrafish using CRISPR/Cas9. *Genome Res.* **25**, 1030-1042. doi:10.1101/gr.186379.114
- Weber, U., Rodriguez, E., Martignetti, J. and Mlodzik, M.** (2014). Luna, a *Drosophila* KLF6/KLF7, is maternally required for synchronized nuclear and centrosome cycles in the preblastoderm embryo. *PLoS ONE* **9**, e96933. doi:10.1371/journal.pone.0096933
- Whelan, N. V., Kocot, K. M., Moroz, T. P., Mukherjee, K., Williams, P., Paulay, G., Moroz, L. L. and Halanych, K. M.** (2017). Ctenophore relationships and their placement as the sister group to all other animals. *Nat. Ecol. Evol.* **1**, 1737-1746. doi:10.1038/s41559-017-0331-3
- Wu, R. S., Lam, I. I., Clay, H., Duong, D. N., Deo, R. C. and Coughlin, S. R.** (2018a). A rapid method for directed gene knockout for screening in G0 zebrafish. *Dev. Cell* **46**, 112-125.e4. doi:10.1016/j.devcel.2018.06.003
- Wu, X., Chen, Z., Gao, Y., Wang, L., Sun, X., Jin, Y. and Liu, W.** (2018b). The krüppel-like factor Dar1 restricts the proliferation of *Drosophila* intestinal stem cells. *FEBS J.* **285**, 3945-3958. doi:10.1111/febs.14652
- Xiao, A., Cheng, Z., Kong, L., Zhu, Z., Lin, S., Gao, G. and Zhang, B.** (2014). CasOT: a genome-wide Cas9/gRNA off-target searching tool. *Bioinformatics* **30**, 1180-1182. doi:10.1093/bioinformatics/btt764
- Yamada, A., Martindale, M. Q., Fukui, A. and Tochinai, S.** (2010). Highly conserved functions of the *Brachyury* gene on morphogenetic movements: insight from the early-diverging phylum Ctenophora. *Dev. Biol.* **339**, 212-222. doi:10.1016/j.ydbio.2009.12.019

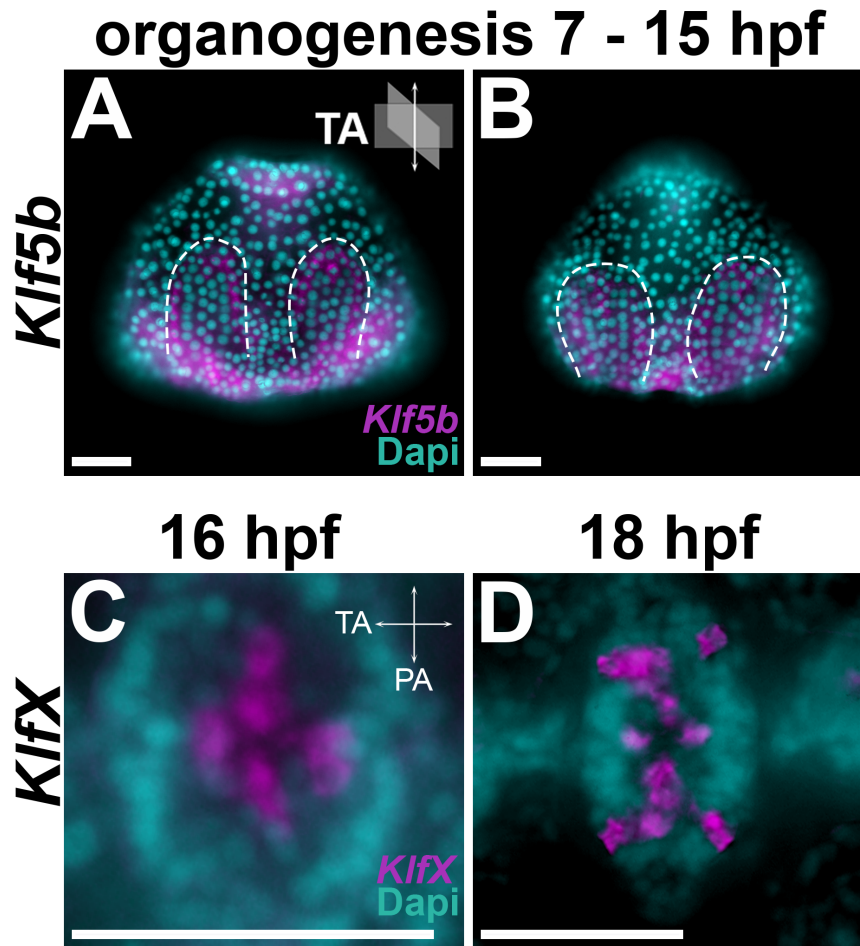


**Fig. S1. Additional *Klf5b* and *KlfX* transcript expression domains.** Schematic depiction of tentacular axis (TA) and pharyngeal axis (PA) orientation are located in panel upper right. (**A**, **B**) Organogenesis stage 7-15 hpf embryos, lateral view, oral up. Dashed lines bound *Klf5b* ectodermal expression (magenta) in rapidly dividing cells (compare with **Fig. S6C**, **G**) that flank developing ctenere row pairs (visible as aligned columns of DAPI stained nuclei bounded by *Klf5b* expression). (**C**, **D**) Magnified aboral views of *KlfX* expression (magenta) in epithelial floor cells of the apical organ. (**C**) Initially *KlfX* expression is detected at 16 hpf in four small clusters of cells at the boundary of each developing embryonic quadrant converging in the center of the apical organ. (**D**) Expression of *KlfX* resolves into several cell clusters by 18 hpf in both the tentacular (TA) and pharyngeal (PA) axes. Scale bars: 50  $\mu$ m.

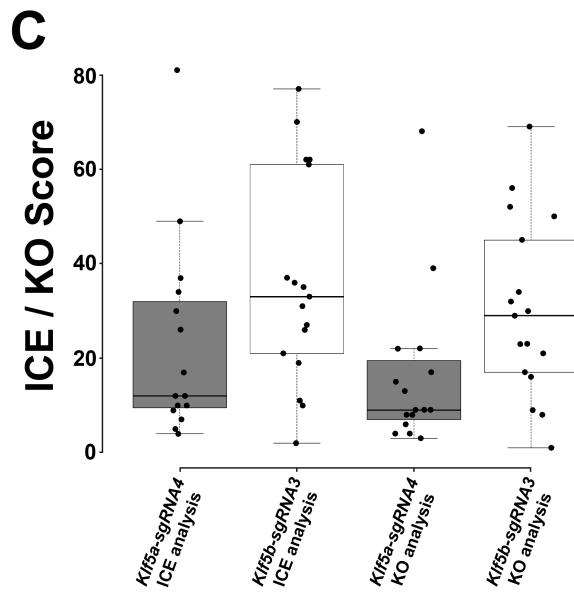
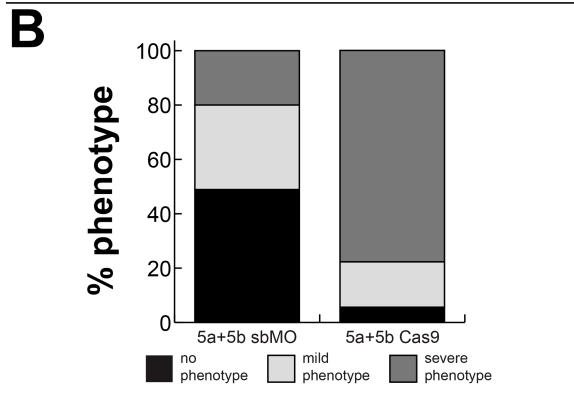
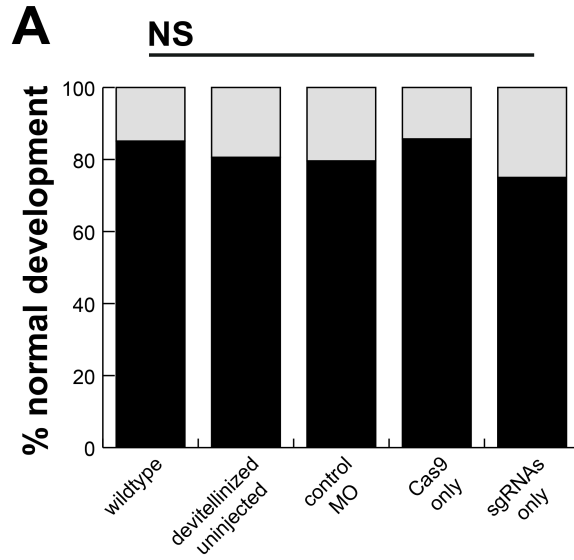


**Fig. S2. Injection quantification and ICE analysis of KLF-Cas9**

(A) Sham injection has no effect on embryonic development. Bar graph comparison of percentage of normal development in wildtype  $n = 161$  (24 abnormal); de-vitellinized but uninjected  $n = 217$  (42 abnormal), two-tailed Fisher's exact test  $P=0.2761$ ; control MO injected  $n = 49$  (10 abnormal), two-tailed Fisher's exact test  $P=0.379$ ; Cas9 only injected  $n = 7$  (1 abnormal), two-tailed Fisher's exact test  $P=1$ ; sgRNA only injected  $n = 4$  (1 abnormal), two-tailed Fisher's exact test  $P=0.4851$ . (B) Comparison of phenotypic proportions in KLF-MO embryos (51% no phenotype, 29% mild phenotype, 20% severe phenotype,  $n = 45$ ) vs KLF-Cas9 embryos (6% no phenotype, 19% mild phenotype, 75% severe phenotype,  $n = 17$ ). (C) Distribution of ICE scores (estimate of indel proportion in signal trace from genomic DNA of individual KLF-Cas9 embryos) and KO scores (estimate of indel proportion that result in frameshift mutation) for *Klf5a-sgRNA4* ( $n = 14$ ) and *Klf5b-sgRNA3* ( $n = 17$ ). Cas9 cut sites were PCR amplified from genomic DNA prepared from individual KLF-Cas9 embryos and subsequently Sanger sequenced. Each cut site data point represents Sanger trace analyses from an individual embryo. Box plot center lines show the median, box limit at 25th and 75th percentiles, whiskers extend 1.5 times interquartile range from the 25th and 75th percentiles, data points are plotted as open circles.



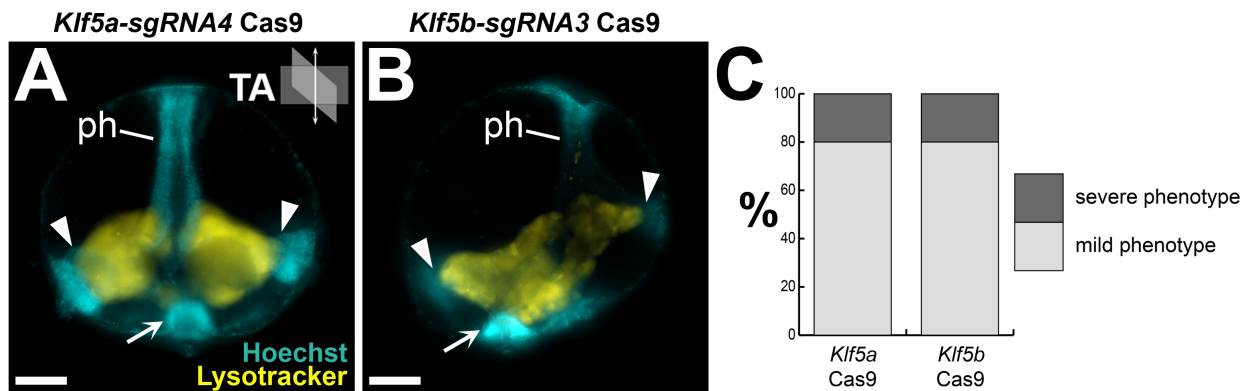


**Fig. S3. Cas9 mediated genome editing of either *Klf5a* or *Klf5b* resulted in reduced phenotype penetrance.** Schematic depiction of tentacular axis (TA) orientation located in panel upper right. Lateral view, oral up. Single gene editing produced primarily mild phenotypes for both *Klf5a* KLF-Cas9 embryos (**A**) and *Klf5b* KLF-Cas9 embryos (**B**). (**C**) Bar graph comparison of distribution of mild (gray) vs severe (black) phenotypes in *Klf5a* KLF-Cas9 embryos ( $n = 5$ , 80% mild) and *Klf5b* KLF-Cas9 embryos ( $n = 5$ , 80% mild). Scale bars: 50  $\mu$ m.

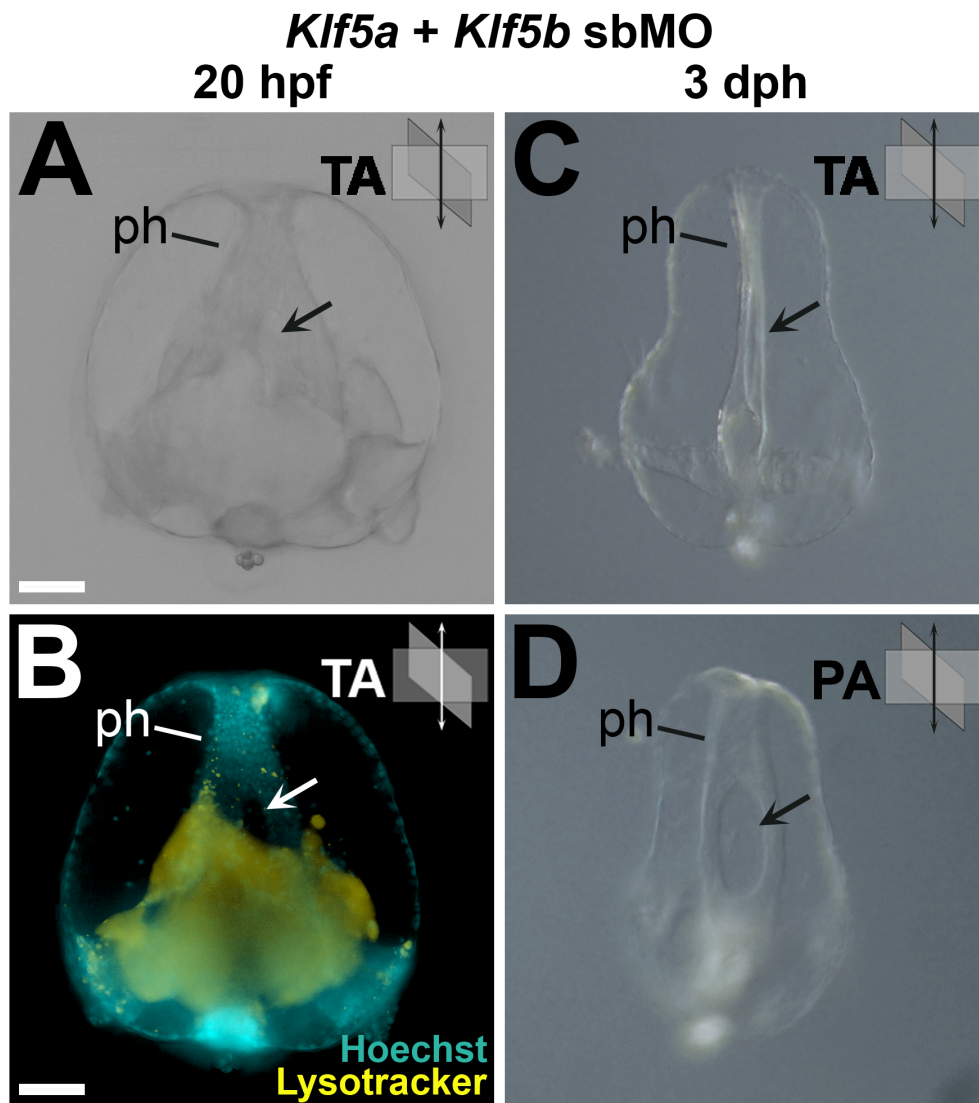


**Fig. S4. Aberrant pharyngeal patterning.** Schematic depiction of tentacular axis (TA) and pharyngeal axis (PA) orientation located in panel upper right. Lateral views, oral up. (**A, B**) 20 hpf double gene KLF-MO embryo with bifurcated (arrow) pharynx (ph). (**C, D**) Same individual KLF-MO embryo 3 days post fertilization (dph) showing persistence of pharyngeal bifurcation patterning defect just anterior of the pharyngeal-gastrovascular junction resulting in a deletion of the pharyngeal folds. Scale bars: 50  $\mu$ m.

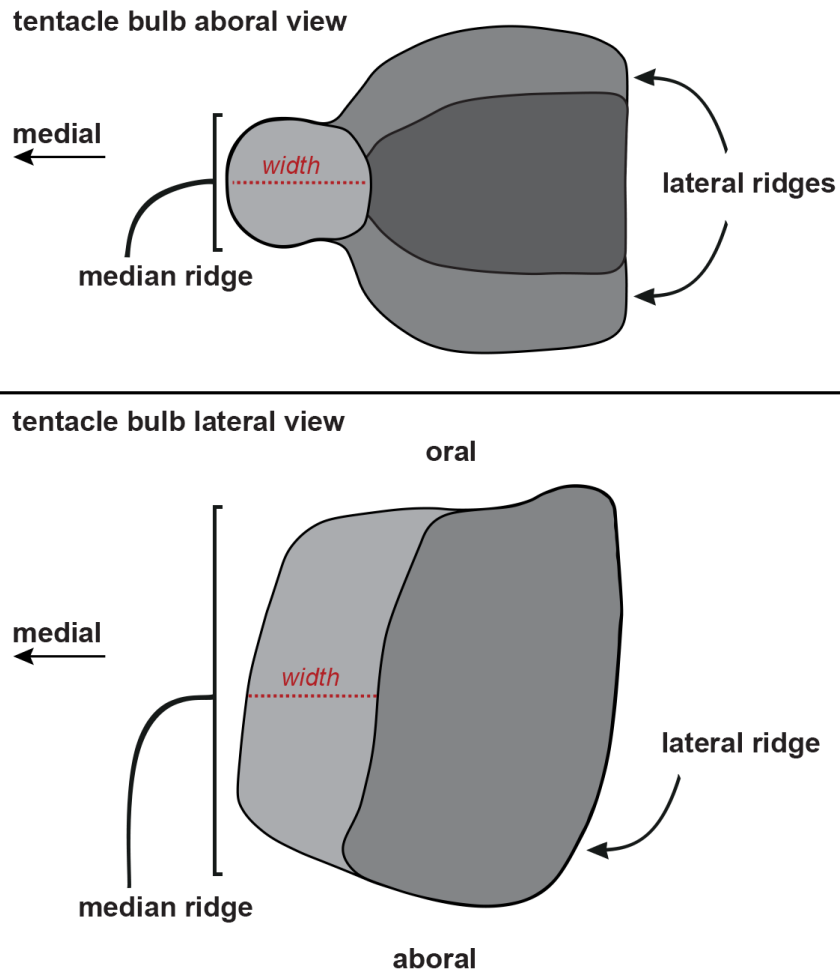


**Fig. S5. Cydippid tentacle bulb schematic.** Aboral view: top; Lateral view: bottom. Tentacular median ridge colored light gray. Tentacular lateral ridges colored darker gray. Tentacle (not shown) is rooted at the aboral medial base of the tentacle bulb. Location of measurement taken for the tentacular median ridge width (refer to Fig. 4N) is denoted with a red dashed line.

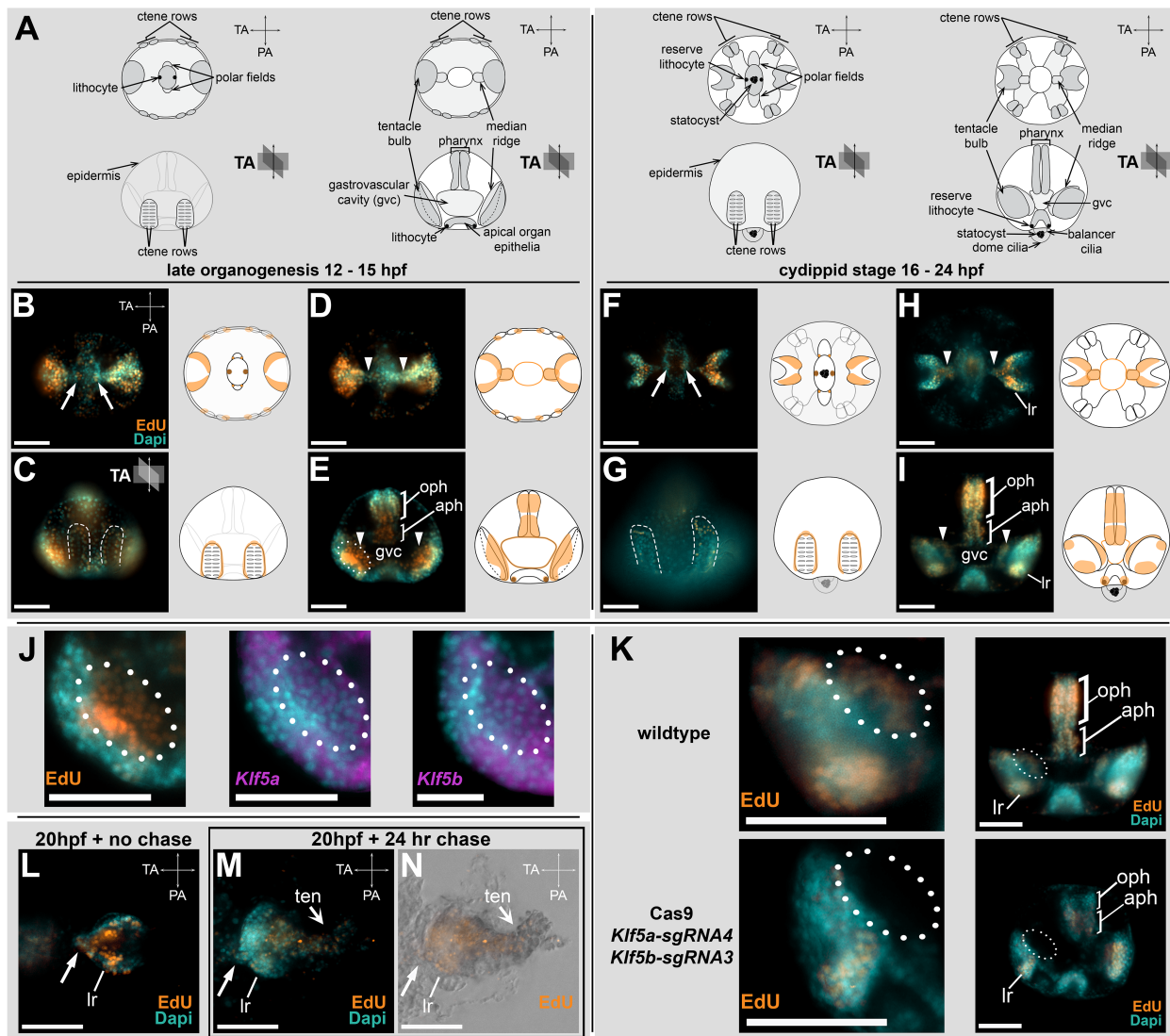


**Fig. S6. Regions of rapid cell proliferation.** (A) Schematics highlighting major morphological landmarks (e.g., ctene rows, pharynx, tentacle bulbs, apical organ) during *M. leidy* embryogenesis. The top row is an aboral view. The bottom row is a lateral view with oral up and aboral down. Schematic depiction of tentacular axis (TA) and pharyngeal axis (PA) orientation are located in panel upper right. (B-I) Edu incorporation after 25 min pulse during embryogenesis. Orientation follows schematics from A. Aboral views in B,D,F,H,L. Lateral views in C,E,G,I,J,K. Edu incorporation is localized to two cell clusters in the apical organ (B,F), epithelial cells flanking the developing ctene rows bounded by dashed lines (C,G), epithelial cells lining the gastrovascular cavity (gvc) (E,I) in the developing tentacular median ridges (arrowheads), and the oral (oph) and aboral (aph) regions of the pharynx (E). (H,I) Later in development, Edu incorporation is found in the tentacular median ridge (arrowheads) and lateral ridges (lr) of the tentacle bulbs and in both oral (oph) and aboral (aph) regions of the pharynx. (J) Region of interest centered on developing tentacle bulbs from ~14 hpf embryos, showing Edu labeling and *Klf5a* and *Klf5b* gene expression within the presumptive tentacular median ridge (outlined). (K, left column) Region of interest centered on ~20 hpf wildtype and KLF-Cas9 embryo tentacle bulbs highlighting loss of Edu labeling in the tentacular median ridge (outlined) in mutants. (K, right column) Whole mount ~20 hpf wildtype and KLF-Cas9 embryo ( $n = 2$ ) showing loss of Edu signal in aboral and oral portions of the pharynx (aph, oph), apical organ, and tentacular median ridge of tentacle bulbs (dashed outline). Note that lateral ridge (lr) cell proliferation is mostly unaffected in KLF-Cas9 embryos. (L) Tentacle bulb after 25 min pulse:0 min chase. (M,N) Tentacle bulb after 25 min pulse:24 hr chase - Edu incorporation is primarily detected in emergent tentacle muscle cells. Scale bars: 50  $\mu$ m. TA, tentacular axis; PA, pharyngeal axis.